Summer 2023

The Synthesis of Novel Rare Earth Thiosilicates Using the Boron Chalcogen Mixture Method for an Interest in Their Magnetic and Optical Properties

Adam Alexander King

Recommended Citation

King, A. A.(2023). *The Synthesis of Novel Rare Earth Thiosilicates Using the Boron Chalcogen Mixture Method for an Interest in Their Magnetic and Optical Properties.* (Master's thesis). Retrieved from https://scholarcommons.sc.edu/etd/7505

The Synthesis of Novel Rare Earth Thiosilicates Using the Boron Chalcogen Mixture Method for an Interest in Their Magnetic and Optical Properties

By

Adam Alexander King

Bachelor of Science
University of South Carolina, 2021

Submitted in Partial Fulfillment of the Requirements

For the Degree of Master of Science in

Chemistry

College of Arts and Sciences

University of South Carolina

2021

Accepted By

Hans Conrad zur Loye, Director of Thesis

Sheryl Wiskur, Reader

Ann Vail, Dean of the Graduate School

Acknowledgements

When I first joined the graduate program, and begun my journey into graduate level chemistry, I had no idea what to expect. I questioned if I could really pass the classes, do the research, and overall learn the chemistry. This was until I joined the zur Loye group, they instilled in me the fundamentals of inorganic chemistry and gave me the confidence to learn chemistry at a higher level. So, I would like to thank Dr. zur Loye, and each member of the zur Loye group for taking me under their wing and helping me become a better chemist. A special thanks to Logan Breton who was fully a mentor to me, teaching me the ins and outs of the lab as well as synthetic crystal chemistry. If it was not for him, I would have never been able to learn how to do the physical research it takes to be a graduate student. I would also like to thank my family who have always supported me throughout my every decision. When I made mistakes, they have always been there to pick me back up, and when I am successful, they are my biggest fans and the first to cheer me on, I love you mom, dad and Grace. Finally, I want to thank my girlfriend and best friend Payton, the only person who has seen my entire process of graduate school, the goods and the bads. She has always been there to support me and give me advice when I need it. I would not have been able to make it this far without her.

Abstract

The chalcogens or the group sixteen elements excluding oxygen, are of interest due to their wide variety of structures and compositions, which gives the potential for a plethora of desired physical properties. This is due to their increased ability to catenate, forming stable chalcogen-chalcogen bonds. When the chalcogens combine with certain main group elements and transition metals they form anionic framework building blocks known as chalcometallates. One such chalcometallate of interest is the thiosilicates, compounds containing Si-S bonds as the anionic frameworks. These compounds are of interest due to their potentials in both their optical and magnetic properties. However, traditional synthesis of chalcogenide compounds has always been plagued by many difficulties. These difficulties include long reaction times, the necessary use of glove boxes, the need for oxygen free starting reagents, and oxide impurities in the product.

A new method for the synthesis of chalcogen containing compounds, The Boron Chalcogen Mixture (BCM) method has also emerged in recent literature. The BCM method tackles many of these longstanding issues in traditional thiosilicate synthesis. This has allowed for a rapid increase in the synthesis and analyzation of these thiosilicate compounds. This work proves the effectiveness of the BCM method in the synthesis of novel thiosilicate compounds, all while analyzing the properties these compounds exhibit for potential industrial use. By using the BCM method with traditional synthetic methods, we have been able to synthesize over 30 novel thiosilicate compounds, solving their unique crystal structures, and analyzing both their magnetic and optical properties.

Table of Contents

LIST OF TABLES

LIST OF FIGURES

LIST OF SYMBOLS

K	Kelvin
$^{\circ}$C	Degrees Celsius
$^{\circ}$	Degrees
λ	Wavelength, normally expressed in nanometers
ν	Frequency, normally expressed in cm-1
Å	Angstrom
$K\alpha$	X-ray emission due to electron transition from a 2p → 1s orbital
2θ	Diffraction angle
Z	Number of formula units
F	Structure factor
F 2	The structure factor squared
R	Residual factor
R_1	Residual factor for refinement against F
wR_2	Residual factor for refinement against F 2
R_{int}	Merging error; a measure of the precision/reproducibility
μ_B	Bohr magneton, a constant quantifying the magnitude of a magnetic moment
μ_{eff}	Effective magnetic moment
T_n	Neal temperature
θ	Weiss Temperature

LIST OF ABBREVIATIONS

CIF	Crystallographic Information File
EDS	Energy Dispersive Spectroscopy
XRD	X-ray Diffraction
PXRD	Powder X-ray Diffraction
SXRD	Single Crystal X-ray Diffraction
SEM	Scanning Electron Microscopy
UV-Vis	Ultraviolet-Visible Spectroscopy
PL	Photoluminescence
FC	Field Cooled
ZFC	Zero-Field Cooled
SQUID	Superconducting Quantum Interference Device
BCM	Boron-Chalcogen Mixture
NLO	Nonlinear Optical Spectroscopy
SHG	Second Harmonic Generation
OQMD	Open Quantum Material Database
FU	Formula Units
ICSD	Inorganic Crystal Structure Database
WPPF	Whole Powder Pattern Fit

LIST OF COMPOUNDS BY CHAPTER

CHAPTER 1

Introduction

The world as we know it continues to evolve and grow every day. New and innovative research is being performed in every aspect imaginable as human society continues to advance at an exponential rate. In fact, there are so many interesting and impressively advanced ideas circulating, that it can be very easy to forget about the basic building blocks for this advancement. That basic building block being chemistry, without which the understanding of what the world is today would not be possible. A specific aspect of chemistry that can be underestimated in its importance is the synthesis of new materials. All materials being used in everyday life were once undiscovered materials with no knowledge of their potentials. So, even though it is not necessarily always considered, the discovery of these new materials continues to be the backbone of human research and advancement. The ability to create new materials is done through the manipulations of chemical bonds, mainly achieved through thermodynamic and kinetic parameters. As new materials are synthesized this also develops scientific understanding of the manipulation of chemical bonds, thus making for the development of better understood and more efficient synthetic routes to obtain these materials. For inorganic materials, exploratory crystal growth is the frontier of novel materials development as it is utilized to analyze both structural and compositional phases of novel compounds and allows for precise atomic structure determination. Exploratory crystal growth uses a variety of crystal growing methods and experimental parameters to obtain a target product. The methods and parameters being chosen are based on the desired product. For certain characterization techniques such as second harmonic generation (SHG) measurements, bulk samples are necessary, while for others, such as single crystal X-ray diffraction (SXRD), high quality, well-faceted single crystals are needed.

Solid State Synthesis

The solid-state synthetic technique involves the reaction of reagents in their solid state. These reactions require the grinding of reagents as well as high reaction temperatures to achieve the desired products. The grinding of reagents is performed to achieve interatomic mixing, while the higher temperature causes thermal motion, that is the diffusion of atoms. Solid-state synthesis is a very sensitive technique due to the many parameters that can affect the product. Stoichiometry, the quality of grinding, and even the purity of reagents used can have a major effect of the product formed. Due to the higher temperatures needed for solid state reactions the products tend to be the most thermodynamically stable form and, therefore, many lower temperature kinetically stable products remain undiscovered. Solid-state reaction products are usually polycrystalline powders as opposed to larger single crystals. These polycrystalline powders are not ideal for structure determination; however, it is an approach that can yield phase pure samples for property measurements. The molten flux synthetic technique improves on the diffusion issues of solid-state syntheses, producing X-ray diffraction quality single crystals more suitable for structural determination.

Molten Flux Crystal Growth

The molten flux synthetic technique improves on the diffusion of solid-state synthesis by adding a “liquid” component to the reaction; this component is known as a flux. A flux is a low melting point reagent, commonly an alkali halide salt or alkali polychalcogenide compound that will melt below the desired reaction temperature, dissolving all reagents upon heating, and crystallizing products when cooled. The process begins with nucleation and finishes with the growth of crystals. As it is not possible to routinely follow the events happening as the flux reaction is taking place, these concepts are understood only conceptually. Traditionally the reaction temperature is chosen to be around 100 °C higher than the flux's known melting point, to ensure the entire flux has melted completely. The reaction should then be slow cooled to 100 °C below the melting point of the flux, as this often results in large, and well faceted single crystals. Once this process is finished, the flux must be separated from the desired crystalline products. This can be done via dissolution in common solvents, such as water or methanol. If there is need for a flux with a very low melting point, a eutectic can be created. A eutectic is a combination of fluxes with a lower melting point then either of the individual components. There are a few significant advantages of the molten flux technique, including access to lower temperature kinetic phases that can not be obtained via solid state reactions. Another advantage being not having to grind reagents, as is necessary for traditional solid-state syntheses. This thesis will describe the use of both the solid state and molten flux synthetic techniques for the preparation of new chalcometallate materials.

Chalcogenides and the Chalcometallates

The chalcogens are the group sixteen elements on the periodic table, excluding oxygen. Differences in the chalcogen's and oxygen's chemical character and their properties excludes oxygen from the chalcogen classification. Oxygen is small and highly electronegative, and the chalcogens are larger and less electronegative when compared to oxygen. However, they also have access to d-orbitals, something oxygen does not. Oxygen is a gas at room temperature and abundant in the atmosphere, while the chalcogens are all solids at room temperature. Therefore, when speaking about the chalcogens, most scientist are referencing sulfur, selenium, and tellurium and often denote the chalcogens in chemical formulas with the letter Q. While also classified as a chalcogen, polonium is rare and extremely toxic and is not used in a classical laboratory setting. Oxide synthesis uses commercially available reagents and can be done in air, without the worry of non-oxygen anion impurities in the product. The synthesis of chalcogenide containing compounds, however, faces many issues due to oxygen being abundant in the atmosphere. Many traditional syntheses involve high temperatures which, in the presence of even trace amounts of oxygen, will result in oxide or oxychalcogenide impurities. Attempts to minimize the reagents contact with oxygen include the use of glove boxes, and oxide free starting reagents; however, trace amounts of oxygen are virtually inevitable in the reaction. This makes it very difficult to have consistently repeatable syntheses with pure products. A search in the Inorganic Crystal Structure Database (ICSD) shows 104,767 oxide containing compounds, but only 35,260 chalcogenide containing compounds. Even with these difficulties, the synthesis of new chalcogenides is still heavily pursued and of great interest. This is mainly due to the chalcogens increased ability to catenate, that is to form stable Q-Q bonds. These catenated bonds increase the variety of structure motifs available. A known motif of interests is the complex anionic frameworks known as the chalcometallates. A chalcometallate is the combination of certain early transition metals and main group elements with a chalcogen (e.g. $[P_2Se_6]^{4-}$, $[P_3Se_7]^{3-}$, $[P_2Se_8]^{2-}$, $[P_8Se_{18}]^{6-}$, $[GeS_4]^{4-}$, $[GeSe_5]^{4-}$, $[Ge_2Se_6]^{6-}$), see figure 1.1. [1]

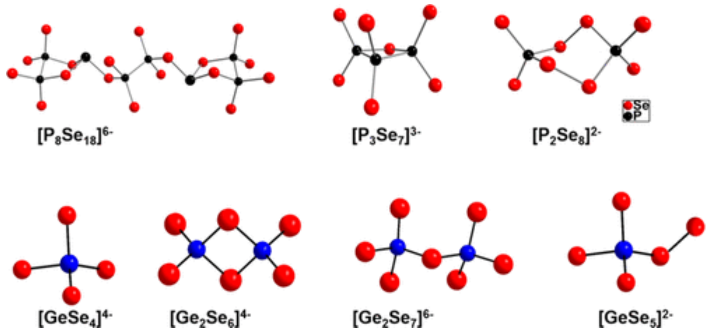

Figure 1.1 Chalcogenide anions that have the ability to form complex frameworks

The chalcometallates were first investigated in the early 1970s when Krebs demonstrated that hydrated orthometalates $A_4MQ_4{\cdot}H_2O$ (A= Alkali Metals; M=Ge, Sn; Q=S, Se) can be isolated from their aqueous solution, consisting of corner or edge-bridged oligomeric units such as $M_2Q_6^{4-}$, $M_2Q_7^{6-}$ or $M_4Q_{10}^{4-}$. [2] Current research on the chalcometallates is motivated by potential technological applications, as they exhibit a variety of desirable properties that have been reported in the literature. A few examples include $Mn_2P_2S_6$ intercalated with an organic dye that possesses both strong nonlinear-optical (NLO) properties and spontaneous magnetization up to a high temperature (Tc ~ 40 K), and $CuInP_2S_6$, which exhibits paraelectric–ferroelectric phase behavior near room temperature and is also being investigated for applications in ultrasonic transducers. [3, 4] While promising results have already been reported, the development of chalcometallate chemistry continues in two main directions. The first being the continued investigation of the known compounds that exhibit these unique properties mentioned above. The second being the development of new synthetic routes and techniques for finding these new materials. The materials presented in this thesis are the thiosilicates (e.g. $[SiS_4]^{4-}$, $[SiS_5]^{4}$), where the silicon is located in a tetrahedral environment; these tetrahedra connect to form anionic frameworks for complex chemical compounds. Thiosilicates have shown promise for their ionic conductivity, nonlinear optical (NLO) properties, optical properties, and magnetic properties. [5–8] $BaLa_2Si_2S_8:Ce^{3+}$ for example, is a cyan emitting phosphor that has the potential to serve as a phosphor in solid-state lighting. [9] Traditionally, thiosilicate synthesis has to address all of the chalcogenide issues mentioned previously. In order to improve the rate at which these compounds can be discovered and analyzed; new synthetic routes have to be explored.

Utilization of Boron in Chalcogenide Synthesis

A synthetic method that was developed in the early 2000s, attempted to address these outstanding problems with traditional chalcogenide synthesis. Wu and Seo took a different approach to typical chalcogenide synthesis, using an oxyphilic reagent to extract the oxygen from the reaction. [10] They hypothesized that by using boron sulfides in their reaction with sulfur, the boron would act as an "oxygen sponge" creating B_2O_3 *in-situ* and allowing for the sulfur to react with the rest of the reagents, as is shown schematically in figure 1.2.

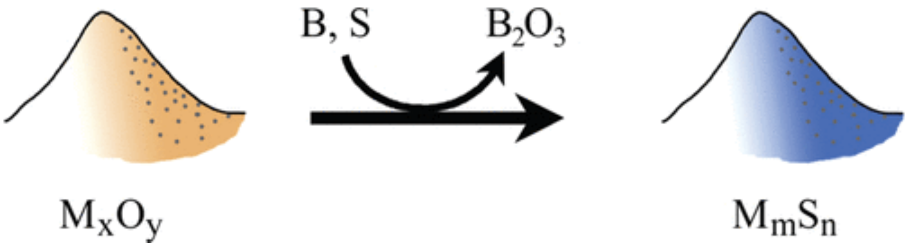

Figure 1.2 *In-Situ* synthesis of Metal sulfidies utilizing B_20_3 [10]

When heated, boron has a higher propensity to form stable boron oxide, i.e., B_2O_3 (-1182.5 kJ/mol) than boron chalcogenide, i.e. B_2S_3 (-247.6kJ/mol), which helps with the sulfidation of various metal oxides. They utilized the approach to synthesize binary metal polysulfides from metal oxide starting materials, proving their hypothesis correct. [10] This method bypassed the traditional issues plaguing sulfide synthesis, as oxygen could now not only be in the reaction vessel, but also be a part of the reagents, and pure sulfide products could still be obtained. Wu continued the advancement of this method when he used it to synthesize rare earth oxysulfides. He demonstrated that by varying the molar ratio of the oxygen containing reagent with the amount of boron and sulfur present in the reaction, the product can be controlled. By using a ratio of 6:2:6 and 6:2:3 of $Ln(OH)_3$, B, and S he was able to synthesize oxysulfide products. However, by decreasing the amount of $Ln(OH)_3$ to a molar ratio of 2, he obtained a pure sulfide product. [11] This added the ability to predict products from reactants using this method, creating a much more effective synthesis of sulfides, that embedded into it a repeatability which had yet to be seen in all of chalcogenide chemistry. However, these were only demonstrations of what could be done utilizing boron in chalcogenide synthesis, the next step was to advance this method through research showing the many possibilities it adds to chalcogenide synthesis.

The Boron Chalcogen Mixture (BCM) Method

The next major breakthrough that tests the limitations of boron chalcogen synthesis is the BCM method. Actinide chalcogenide research is of interest due to chemical compositions and actinide oxidation states available in these compounds, unique oxidation states allowing for the study of the 5f electron. However, actinide oxides are extremely stable and thus actinide oxide impurities often occur and dominate synthetic attempts to create actinide chalcogenides. The BCM method applies Wu and Seo's boron sulfide reaction with actinide oxide reagents and successfully synthesizes phase pure actinide sulfides. This successful synthesis is illustrated in figure 1.3.

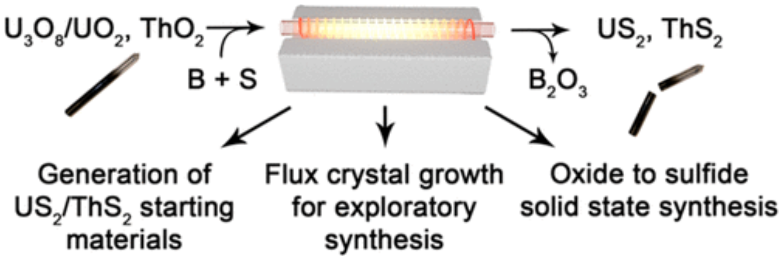

Figure 1.3: BCM method reaction profile for an actinide oxide to actinide chalcogenide reaction

The BCM method also improves on the utilization of boron in chalcogenide reagents in several ways. [12] The publication of the BCM method, was the first to analyze the temperature at which sulfurization occurs, as can be seen in figure 1.4. This paper also shows the use of boron as on oxyphilic reagent that in the presence of other chalcogenides, selenium, and tellurium and uranium and thorium, creates uranium and thorium selenid es and tellurides. The temperature dependence of sulfurization was also analyzed using the BCM method which is shown for both uranium and thorium in figure 1.4. [12]

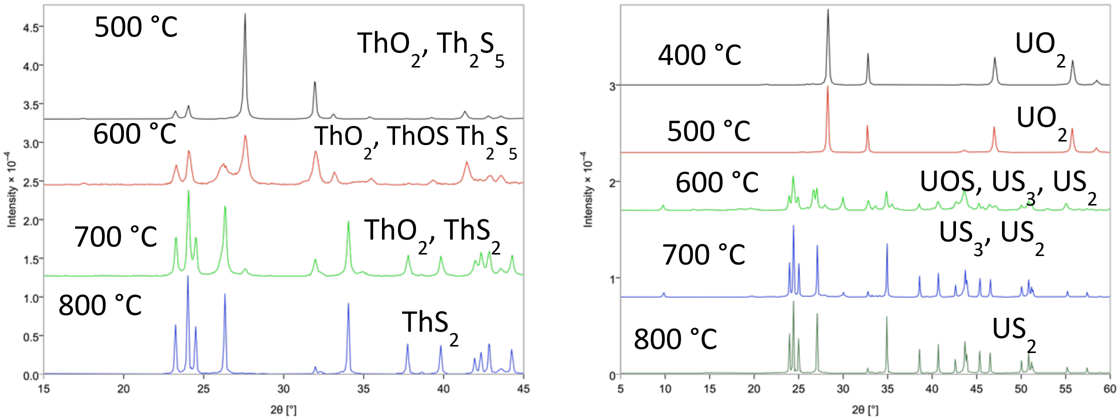

Figure 1.4. Temperature dependence of sulfurization for uranium and thorium sulfides

The BCM method has been applied to the chalcometallates as well. In the literature, lanthanide thioborates, $LnBS_3$ (Ln= La, Ce, Pr, Nd) were researched as a potential NLO material and a recent paper demonstrated the potential of the BCM method in the realm of chalcometallate materials as also being able to incorporate boron in the product while still using oxide starting materials. [13]

Reaction Set Up

Chalcometallate reactions using a combination of the BCM and flux method can be weighed out in air and allow for the use of oxide starting reagents. [12] This includes commercially available Ln_2O_3 and SiO_2, where in the past Ln_2S_3 and elemental silicon would have to be used. Ln_2S_3 is not commercially available and has to be made in-house for each rare earth that is desired to be used. This can be done by the decomposition of ammonium thiocyanate into $CS_2 + H_2S + NH_2$. H_2S is then passed over Ln_2O_3 (s) using argon as a carrier gas at 1050 ˚C resulting in pure products of Ln_2S_3 (s) and $3{\cdot}H_2O$ (g). The reaction set up can be seen in figure 1.5. Once reagents are acquired, they are added to a fused silica or quartz tube as the reaction vessel. For typical reactions using quartz tubes they must be carbon coated to avoid the silicon oxide in the tube wall from reacting with the reagents.

Figure 1.5. Reaction set up for synthesizing Ln_2S_3

Carbon coating is the process of decomposing acetone onto the tube wall to essential coat it in carbon, creating a layer between the silicon oxide in the glass and the reagents, thus keeping them from reacting with each other. An advantage of thiosilicates and the BCM method is that regular quartz tubes can be used and do not have to be carbon coated, as the silicon oxide is already a part of the reactants. These tubes are evacuated to 10^{-4} millitorr and flame sealed using a methane/oxygen flame torch. The sealed tube is then placed in a programmable furnace and set to run at the selected reaction parameters.

Thiosilicate Properties

As shown previously the chalcometallates and, in particular thiosilicates, have shown potential for their variety of desirable properties such as ionic conductivity, NLO and magnetic properties. The zur Loye group, has mainly focused on the optical and magnetic properties of chalcogenide containing compounds. [12-15] As with our previous interest, we focused on analyzing these same properties of the thiosilicates as well. There are numerous examples of thiosilicate publications in the literature that discuss the two main optical properties of interest, namely their nonlinear optical (NLO) behavior, mainly their Second Harmonic Generation (SHG) abilities and their photoluminescence. SHG is a NLO process that involves the frequency doubling of a photon by a noncentrosymmetric structure. A noncentrosymmetric structure being a structure featuring no inversion center. When two photons of frequency “X” and wavelength “Y” interact with a structure that is SHG active, the photons generate a new photon with a frequency of “2X” and wavelength of “$\frac{1}{2}$Y”. An important measurement of second harmonic generation is phase matching, or a condition where the polarization wave produced by two photons in a NLO medium has the same phase velocity as a free wave of the same frequency. The process for achieving this is a technique called birefringent phase matching, where the birefringence of a nonlinear crystal is exploited. Birefringence is the property of some transparent materials where the refractive index depends on the polarization direction. There are two common forms of birefringent phase matching. The first being noncritical phase matching where the beam is propagated along an axis of an index ellipsoid. The other form is critical phase matching. This is where the angular dependence of the refractive index is exploited. Another difference in phase matching comes from the polarized states. In Type I two photons with ordinary polarization will combine to double the frequency and extraordinary polarization. In Type II, two photons with orthogonal polarization will combine to double the frequency and ordinary polarization. For a single crystal orientation there can only be one type of critical phase matching. Trends in thiosilicate crystallization has shown that they tend to prefer noncentrosymmetric space groups and as such can exhibit NLO properties, such as second harmonic generation.

Another optical property commonly sought after in new materials is photoluminescence. Photoluminescence is the emission of visible light after the absorption of photons, commonly UV light. Photoluminescence can occur in two ways, the first being fluorescence and the second being phosphorescence. Both begin with the excitation step, which is the excitation of a ground state electron to a singlet excited state resulting from the absorption of a photon. Once in its excited state, the electron is unstable and wants to return to its ground state. It will attempt to do this by first relaxing through the excited states vibrational levels, a process known as vibrational relaxation. Once at the lowest vibrational level of the first singlet excited state, the electron can either undergo fluorescence or intersystem crossing. Fluorescence is the deexcitation from the first singlet excited state back down to the ground state, an extremely fast process, about 10^{-8} seconds long. The energy from this jump is emitted as visible light. Intersystem crossing involves the change from the singlet excited state to the triplet excited state. In the singlet state, an electron pair is spin up and spin down, however in the triplet state they have the same spin direction. As the excited electron must be flipped on deexcitation, this is considered a spin forbidden transition. This does not mean intersystem crossing won't happen, but that it occurs much more slowly than a spin allowed transition. After intersystem crossing occurs, the electron goes through vibrational relaxation until it gets to the lowest vibrational level of the first excited triplet state. The jump from the first excited triplet state to singlet ground state is known as phosphorescence. The difference between phosphorescence and fluorescence is the speed at which they occur. Due to the electrons again having to flip from the same orientation in the triplet state to opposite orientations in the singlet state, phosphorescence is a spin forbidden transition, unlike fluorescence which is spin allowed, making it much slower process than fluorescence. Therefore, when both are analyzed under UV light it is common for phosphorescent materials to emit a glow even after the light is turned off, while fluorescent materials will immediately stop emitting when the UV light is turned off.

The final property we in the zur Loye lab wanted to analyze in the thiosilicates is their magnetic behavior. Magnetism stems from the presence of unpaired electrons, whose spins at higher temperatures will be thermally randomized. In this condition they are referred to as being paramagnetic. As these electrons are cooled down, they have the potential to order magnetically in certain ways. Two common types of magnetic order are ferromagnetism and antiferromagnetism. Ferromagnetism occurs when the electrons align spin parallel, while antiferromagnetism occurs when the electrons align spin antiparallel. The magnetic moment of a material can be extracted from the magnetic data by using the Curie-Weiss law. The Curie-Weiss law is $X = \frac{C}{(T-\theta)}$, where X is the magnetic susceptibility, C is the Curie constant, T is the absolute temperature and θ is the Weiss constant. Information is extracted from this data by plotting either the magnetic susceptibility or the inverse susceptibility vs the temperature. In such plots the magnetic transitions can readily be observed, and from the straight line portion of the inverse susceptibility vs temperature plot, the effective magnetic moment can be calculated. The antiferromagnetic transition temperature is known as the Neal Temperature (T_N) while the ferromagnetic transition temperature is known as the Curie Temperature (T_C). These are also the two types of magnetic behavior that we will investigate the thiosilicate compounds for.

Thiosilicate units by themselves however have no unpaired electrons and thus no potential magnetic ordering. Due to their ability to create a variety of structural motifs they are able to incorporate a number of different elements into their structures. This includes the rare earths and transition metals, both of which can have unpaired electrons depending on their oxidation states, and thus can give rise to potential magnetic order.

The research goal discussed in this thesis was to take advantage of the structural abilities of thiosilicates and to incorporate additional elements to impart physical properties of interest, such as optical and magnetic properties. To achieve these goals the BCM method was utilized in this research project. The results of these efforts are illustrated herein through a multitude of different structural and compositional variation of thiosilicate compounds that were successfully synthesized using the BCM method and analyzed for the desired properties. As can be seen from table 1.1, over 40 novel rare earth containing thiosilicates have been successfully synthesized using the BCM method in less than two years of exploring these compounds in the zur Loye group. This thesis will focus on the process of this research by describing numerous compounds that, each uniquely, presented different synthetic challenges. Furthermore, the structural and physical property characterization of these materials will be discussed.

Table 1.1. Family of rare earth thiosilicates my research has focused on. Green shows novel compounds I have synthesized. Red shows potential target compositions for future synthesis. Blue shows reported compounds in the literature

Ln^{3+} M^{2+}	La	Ce	Pr	Nd	Sm	Gd	Tb	Dy	Ho	Er	Tm	Yb
Mg	🟦	🟩	🟩	🟩	🟩	🟩	🟩	🟩	🟩	🟩	🟥	🟥
Cr	🟦	🟥	🟥	🟥	🟩	🟥	🟥	🟥	🟥	🟥	🟥	🟥
Fe	🟦	🟥	🟥	🟥	🟥	🟩	🟩	🟩	🟩	🟩	🟩	🟩
Co	🟦	🟥	🟥	🟥	🟥	🟩	🟩	🟩	🟩	🟩	🟩	🟩
Ni	🟦	🟥	🟥	🟥	🟥	🟩	🟩	🟩	🟩	🟩	🟩	🟩

References

1. Kanatzidis, M. G. Discovery-Synthesis, Design, and Prediction of Chalcogenide Phases. *Inorg. Chem.* ***2017,*** *56, 3158-3173.*
2. Krebs, B. Thio- and Seleno-Compounds of Main Group Elements Novel Inorganic Oligomers and Polymers. *Angew. Chem. Int. Ed. Engl.* ***1983,*** *22, 113-134.*
3. Dziaugys, A.; Banys, J.; Macutkevic, J.; Sobiestianskas, R.; Vysochanskii, Y. Dipolar glass phase in ferrielectrics: CuInP$_2$S$_6$ and Ag$_{0.1}$Cu$_{0.9}$InP$_2$ S$_6$crystal. *Physica. Status. Solidi (a).* ***2010,*** *207, 1960-1967.*
4. Lacroix, P. G.; Clément, R.; Nakatani, K.; Zyss, J.; Ledoux, I. Stilbazolium-MPS$_3$ Nanocomposites with Large Second-Order Optical Nonlinearity and Permanent Magnetization. *Science.* ***1994,*** *263, 658-660.*
5. Gauthier, G.; Jobic, S.; Evain, M.; Koo, H.-J.; Whangbo, M.-H.; Fouassier, C.; Brec, R. Syntheses, Structures, and Optical Properties of Yellow Ce$_2$SiS$_5$, Ce$_6$Si$_4$S$_{17}$, and Ce$_4$Si$_3$S$_{12}$ Materials. *Chem. Mater.* ***2003,*** *15, 828-837.*
6. Huang, W.; Matsui, N.; Hori, S.; Suzuki, K.; Hirayama, M.; Yonemura, M.; Saito, T.; Kamiyama, T.; Sasaki, Y.; Yoon, Y.; Kim, S.; Kanno, R. Anomalously High Ionic Conductivity of Li$_2$SiS$_3$-Type Conductors. *J. Am. Chem. Soc.* ***2022,*** *144, 4989-4994.*
7. Riccardi, R.; Gout, D.; Gauthier, G.; Guillen, F.; Jobic, S; Garcia, A.; Huguenin, D.; Macaudière, P.; Fouassier, C.; Brec, R. Structural Investigation and Luminescence Properties of the Ce$_3$(SiS$_4$)$_2$X (X=Cl, Br, I) Family and the La$_{3-x}$Ce$_x$(SiS$_4$)$_2$I ($0 \le x \le 1$) Solid Solution. *J. Solid State Chem.* ***1999,*** *147, 259-268.*
8. Li, G. M.; Chu, Y.; Li, J.; Zhou, Z. X. Li$_2$CdSiS$_4$, a promising IR NLO material with a balanced E$_g$ and SHG response originating from the effect of Cd with d^{10} configuration. *Dalton Trans.* ***2020,*** *49, 1975-1980.*
9. Lee, S. P.; Chan, T. S.; Chen, T. M. Novel reddish-orange-emitting BaLa$_2$Si$_2$S$_8$:Eu^{2+} thiosilicate phosphor for LED lighting. *ACS Appl Mater Interfaces.* ***2015,*** *7, 40-44.*
10. Wu, L. M.; Seo, D. K. New solid-gas metathetical synthesis of binary metal polysulfides and sulfides at intermediate temperatures: utilization of boron sulfides. *J. Am. Chem. Soc.* ***2004,*** *126, 4676-4681.*
11. Huang, Y.-Z.; Chen, L.; Wu, L.-M. Crystalline Nanowires of Ln$_{2<}$O$_2$S, Ln$_2$O$_2$S$_2$, LnS$_2$ (Ln = La, Nd), and La$_2$O$_2$S:Eu^{3+}. Conversions via the Boron-Sulfur Method That Preserve Shape. *Cryst. Des.* ***2008,*** *8, 739-743.*
12. Breton, L. S.; Klepov, V. V.; zur Loye, H.-C. Facile Oxide to Chalcogenide Conversion for Actinides Using the Boron-Chalcogen Mixture Method. *J. Am. Chem. Soc.* ***2020,*** *142, 14365-143*

13. Breton, L. S.; Morrison, G.; Lacroix, M. R.; Halasyamani, P. S.; zur Loye, H.-C. Lanthanide thioborates, an emerging class of nonlinear optical materials, efficiently synthesized using the boron-chalcogen mixture method. *Chem. Commun. (Camb).* ***2022,*** *58, 7992-7995*
14. Breton, L. S.; Smith, M. D.; zur Loye, H.-C. Trends in Rare Earth Thiophosphate Syntheses: $Rb_3Ln(PS_4)_2$ (Ln = La, Ce, Pr), $Rb_{3-x}Na_xLn(PS_4)_2$ (Ln = Ce, Pr; x = 0.50, 0.55), and $RbEuPS_4$Obtained by Molten Flux Crystal Growth. *CrystEngComm.* ***2021,*** *23, 5241-5248.*
15. Usman, M.; Smith, M. D.; Morrison, G.; Klepov, V. V.; Zhang, W.; Halasyamani, P. S.; zur Loye, H.-C. Molten Alkali Halide Flux Growth of an Extensive Family of Noncentrosymmetric Rare Earth Sulfides: Structure and Magnetic and Optical (SHG) Properties. *Inorg. Chem.* ***2019,*** *58, 8541-8550.*

CHAPTER: 2

Crystal Structures and Property Measurements of Novel Rare Earth Magnesium Thiosilicates Synthesized via Flux Crystal Growth Utilizing the Boron Chalcogenide Mixture Method

Abstract

Nine new rare earth magnesium containing thiosilicates of the formula $RE_3Mg_{.5}SiS_7$ (Ln= Ce, Pr, Nd, Sm, Gd, Tb, Dy, Ho, Er) were synthesized in an alkali halide flux using the Boron Chalcogenide Mixture (BCM) method. Crystals of high quality were produced, and their structures determined by single crystal X-ray diffraction. The compounds crystalize in the hexagonal crystal system in the $P6_3$ space group. Phase pure powders of the compounds were used for magnetic Second Harmonic Generation (SHG) measurements. Magnetic measurements indicate that $Ce_3Mg_{0.5}SiS_7$, $Sm_3Mg_{0.5}SiS_7$, and $Dy_3Mg_{0.5}SiS_7$ exhibit paramagnetic behavior with a negative Weiss temperature over the T=2-300 K temperature range. SHG measurements of $La_3Mg_{0.5}SiS_7$ demonstrated SHG-activity with an efficiency of 0.16 times the standard potassium dihydrogen phosphate (KDP).

Introduction

Metal chalcogenides have become the foundation of many modern technologies due to their structural and compositional diversity, which results in a plethora of desired physical properties.[1] The chalcometallates, one class of chalcogenides, result from the combination of the chalcogens with certain main group elements and that yield complex anionic framework structures. The zur Loye group, utilizing the molten flux synthetic method, has explored the synthesis of single crystals of a variety of chalcometallate materials, including thiophosphates, thiogermanates and thiosilicates, to explore their magnetic and optical properties.[2, 3] A major obstacle to the synthesis of these compounds is the lack of commercially available rare earth sulfide starting materials, which necessitates their preparation in the laboratory prior to exploring the syntheses of chalcometallate compounds. Recently, we have demonstrated the use of the Boron-Chalcogen Mixture (BCM) method to synthesize single crystals of, $LnBS_3$ (Ln= La, Ce, Pr, Nd) and measured their non-linear optical properties.[4] The BCM method allows for the *in-situ* sulfurization of lanthanide oxide starting reagents, thereby avoiding the need for lanthanide sulfide reagents.[5] As this method has been previously used to synthesize a number of lanthanide and transition metal sulfide compounds, we again chose to utilize the BCM method to explore a family of chalcometallates, $RE_3Mg_{0.5}SiS_7$ (RE= rare earth) compounds to investigate their magnetic and optical properties.[6-8]

The $RE_3M_xMQ_7$ (M= metal) family of compounds form an extensive family of quaternary rare-earth chalcogenides due to the unique structural flexibility of the $La_3Mn_{0.5}GeS_7$ structure type that can accommodate a variety of elements that can impart optical and magnetic properties to the material.[9-19] The structural flexibility of this family is a product of the metal atom's ability to have full occupancy taking on a trigonal planar coordination environment, an example being La_3AgSiS_7, or be half occupied taking on a octahedral coordination environment such as $RE_3Cd_{0.5}GeS_7$.[20, 21] The compositional flexibility stemming from a variety of combinations of rare-earths, metals, tetrels and chalcogenides. The metals in these compounds range from groups 1-15 resulting in a staggering number of almost 2000 reported phases.[22] However, a survey of this family of compounds was recently published by Zhou et al. which highlighted the lack of certain elemental compositions within this phase space.[20] One series with minimal reported phases is the rare earth magnesium thiosilicates, $RE_3Mg_{0.5}SiS_7$. The $La_3Mg_{0.5}SiS_7$ and $Y_{0.5}Mg_{0.5}SiS_7$ analogs being the only ones reported.[23, 24]

Due to this, we decided to investigate this series in order to explore the optical and magnetic properties of the rare earth metals in various structural environments. Furthermore, Mg^{2+} is diamagnetic and optically inactive, enabling us to study solely the behavior of the rare earths in these compounds. Many of these compounds, including those presented in this paper, crystallize in the non-centrosymmetric space group $P6_3$, which makes these structures potentially SHG active and, thus, able to exhibit nonlinear optical properties (NLO). To date, the synthesis of the known $RE_3M_xMQ_7$ (M= metal) compounds has primarily been done by solid state synthesis, though a few examples of other synthetic routes exist, such as the molten flux synthesis and arc melted precursors.[25, 26] As the molten flux synthetic technique has shown success, we chose to utilize this combined with the BCM method to grow crystals of the title compounds for structural characterization and, in some cases, also performed solid-state synthesis using the BCM method to create bulk samples. Herein we present the synthesis of high-quality single crystals of $RE_3Mg_{0.5}SiS_7$ (RE=La-Nd, Sm-Er) and the determination of their crystal structures. Furthermore, the magnetic properties of $RE_3Mg_{0.5}SiS_7$ (Ce, Dy, Sm) are investigated and SHG properties of $La_3Mg_{0.5}SiS_7$ are reinvestigated.

Experimental

RE_2O_3 (RE= La, Nd, Sm, Gd, Dy, Ho, Er) (99.9%, Alfa Aesar), CeO_2 (99.9%, Alfa Aesar), Pr_6O_{11} (99.9% Alfa Aesar), Tb_4O_7 (99.9% Alfa Aesar), Sulfur (Fischer Scientific), Boron (99.9%, Beantown Chemical) , SiO_2 (99.9%, Alfa Aesar), NaI (99.9%, Beantown Chemical) NaCl (99.9%, Alfa Aesar) , $CaCl_2$ (Fischer Scientific), and $MgCO_3$ (Allied Chemicals) reagents were used to synthesize the target compounds. MgO was prepared by decomposing $MgCO_3$ at 700 ˚C for 24hrs. Pr_2O_3 and Tb_2O_3 were prepared by the reduction of Pr_6O_{11} and Tb_4O_7 at 1000 °C for 24 hours under a 4% hydrogen flow. The resulting Tb_2O_3 and Pr_2O_3 were stored in a nitrogen glove bag. NaI, NaCl, $CaCl_2$, and MgO were stored overnight in a drying oven set to 260 °C to remove moisture.

$RE_3Mg_{0.5}SiS_7$ (RE=Nd-Er) were synthesized by the addition of RE_2O_3, boron, sulfur, SiO_2, and MgO powders in a 3:20:30:2:1 molar ratio, respectively, into a fused silica tube (10 x 12 mm inner and outer diameters, about 15 cm length) along with 250 mg of NaI flux (75 mg in the case of Nd). The fused silica tube was evacuated to 10^{-4} torr and flame sealed using a methane/oxygen torch. The sealed fused silica tube was placed into a programmable furnace set to heat to 760°C in 20 hours, to dwell at this temperature for 20 hours, and to cool to 560°C in 20 h, at which point the furnace was shut off and allowed to return to room temperature.

$RE_3Mg_{0.5}SiS_7$ (RE=La, Pr) were synthesized using a similar procedure, except for the use of 75 mg of a $CaCl_2$/NaCl eutectic instead of NaI and the reagent mixture was ground using a mortar and pestle prior to the addition of the flux. The tube was heated to 950°C in 20 hours, dwelled at this temperature for 20 hours, cooled to 750°C in 20 hours, at which point the furnace was shut off and allowed to return to room temperature.

$RE_3Mg_{0.5}SiS_7$ (RE=Ce) was obtained using the same synthetic procedures as the RE = La and Pr analogues but with the use of 75 mg of NaCl flux instead of the $CaCl_2$/NaCl eutectic.

To prepare samples for property measurements of $RE_3Mg_{0.5}SiS_7$, traditional solid-state syntheses were preformed using the same materials and molar ratio mentioned above. For these reactions, the reagents were intimately ground. The ground mixture was added to a fused silica tube that was placed into a programmable furnace set to ramp to

950˚C, dwell for 12 hours, at which point the furnace was shut off and allowed to return to room temperature. The powder X-ray diffraction patterns can be seen in Figures 2.1-2.4.

CAUTION: Please note boron sulfides are moisture sensitive and produce H_2S gas on contact with moisture and water. All post reaction work was done in the properly labeled fume hood. Reproduction of the synthesis should be done with the proper safety procedures in place

Single-Crystal X-ray Diffraction (SXRD)

X-ray intensity data of yellowish-brown plate crystals of all title compositions were collected at 300 K using a Bruker D8 QUEST diffractometer equipped with a PHOTON-II area detector and an Incoatec microfocus source (Mo Kα radiation, λ = 0.71073 Å). Single crystals were mounted on a microloop with immersion oil. The raw area detector data frames were reduced and corrected for absorption effects using the SAINT+ and SADABS programs.[27] Final unit cell parameters were determined by the least-squares refinement of a large array of reflections form each data set.[28] An initial structural model was obtained with SHELXT. Subsequent difference Fourier calculations and full-matrix least-squares refinement against F^2 were performed with SHELXL-2018 using the ShelXle interface.[29] All compounds crystalize in the noncentrosymmetric, hexagonal space group $P6_3$, which is uniquely confirmed by the pattern of systematic absences in the intensity data. The asymmetric unit contains three sulfur atoms, one lanthanide atom, one magnesium atom and one silicon atom. All atoms are all located on positions of general crystallographic symmetry. All atoms were refined with anisotropic displacement parameters. The crystallographic data and diffraction results are listed in table 2.1.

Powder X-ray Diffraction (PXRD)

Powder X-ray diffraction (PXRD) data were collected using a powder sample of $RE_3Mg_{0.5}SiS_7$ obtained by the solid-state synthesis. The samples used for property measurements PXRD patterns can be seen below in figures 2.1-2.4. Data were collected on a Bruker D2 PHASER diffractometer using Cu Kα radiation over a 2θ range 10–65° with a step size of 0.02°.

Energy-Dispersive Spectroscopy (EDS)

EDS was performed on single crystal products using a Tescan Vega-3 SEM equipped with a Thermo EDS attachment. The SEM was operated in low-vacuum mode. Crystals were mounted on an SEM stub with carbon tape and analyzed using a 30 kV accelerating voltage and a 100 s accumulation time. SEM images of the crystals can be found in figure 2.5. The obtained EDS spectra for each crystal can be found in table 2.2.

Table 2.1 Crystallographic Data and diffraction results for all reported compounds

Chemical formula	$La_3Mg_{0.5}SiS_7$	$Ce_3Mg_{0.5}SiS_7$	$Pr_3Mg_{0.5}SiS_7$	$Nd_3Mg_{0.5}SiS_7$	$Sm_3Mg_{0.5}SiS_7$
Formula weight	681.40	685.03	687.40	697.39	715.79
Crystal system	Hexagonal				
Space group, Z	*P*6_3	*P*6_3	*P*6_3	*P*6_3	*P*6_3
a, Å	10.35010(10)	10.23860(10)	10.18500(10)	10.1219(13)	10.03110(10)
b, Å	10.35010(10)	10.23860(10)	10.18500(10)	10.1219(13)	10.03110(10)
c, Å	5.74220(10)	5.72220(10)	5.69630(10)	5.6691(11)	5.64820(10)
β, deg.	90	90	90	90	90
V, Å^3	532.719	519.487(14)	511.735(13)	503.00(16)	492.195(13)
ρ_{calcd}, g/cm^3	4.248	4.379	4.461	4.605	4.829
Radiation (λ, Å)	Mo-Kα (0.710173 Å)				
μ, mm^{-1}	13.259	14.405	15.561	16.786	19.227
T, K	399.12	299.09	298.89	298.53	300.2
Crystal dim., mm^3	0.04 x 0.04 x 0.04	0.05 x 0.05 x 0.04	0.05 x 0.05 x 0.05	0.05 x 0.05 x 0.05	0.05 x 0.05 x 0.05
2θ range, deg.	3.938-36.302	2.297-36.259	4.001-36.302	2.323-36.326	2.344-36.341
Reflections collected	22794	22771	22302	22801	21059
Data/parameters/restraints	1737/38/1	1683/38/1	1654/ 38 /1	1636/38/1	1589/38/1
R_{int}	0.0280	0.0280	0.0303	0.0356	0.0308
Goodness of fit	1.165	1.211	1.193	1.132	1.234
$R_1(I > 2\sigma(I))$	0.0077	0.0097	0.0089	0.0085	0.0103
wR_2 (all data)	0.0179	0.0262	0.0206	0.0196	0.0236

Chemical formula	$Gd_3Mg_{0.5}SiS_7$	$Tb_3Mg_{0.5}SiS_7$	$Dy_3Mg_{0.5}SiS_7$	$Ho_3Mg_{0.5}SiS_7$	$Er_3Mg_{0.5}SiS_7$
Formula weight	736.42	741.43	752.17	759.46	766.45
Crystal system	Hexagonal				
Space group, Z	$P6_3$	$P6_3$	$P6_3$	$P6_3$	$P6_3$
a, Å	9.9571(3)	9.8952(5)	9.84310(10)	9.7890(11)	9.75330(10)
b, Å	9.9571(3)	9.8952(5)	9.84310(10)	9.7890(11)	9.75330(10)
c, Å	5.6344(3)	5.6257(4)	5.62710(10)	5.6255(9)	5.63680(10)
β, deg.	90	90	90	90	90
V, Å^3	483.78(4)	477.04(6)	472.149(13)	466.84(13)	464.372(13)
ρ_{calcd}, g/cm^3	5.055	5.162	5.291	5.403	5.481
Radiation (λ, Å)	Mo-Kα (0.710173 Å)				
μ, mm^{-1}	21.918	23.611	25.126	26.826	28.519
T, K	303(2)	299.74	303(2)	297.69	299.32
Crystal dim., mm^3	0.06 x .06 x .04	0.05 x .05 x .05	0.07 x 0.06 x 0.04	0.04 x 0.04 x 0.04	0.05 x 0.05 x 0.04
2θ range, deg.	2.362-40.290	2.377-36.315	2.389-40.265	2.402-36.287	2.411-36.325
Reflections collected	29133	19488	30408	20237	19302
Data/parameters/restraints	2028/38/1	1536/38/1	1998/37/1	1507/38/1	1498/38/1
R_{int}	0.0322	0.0316	0.0324	0.0335	0.0319
Goodness of fit	1.160	1.232	1.25	1.194	1.224
$R_1(I > 2\sigma(I))$	0.0101	0.095	0.0112	0.096	0.0118
wR_2 (all data)	0.0214	0.0229	0.0227	0.0215	0.0270

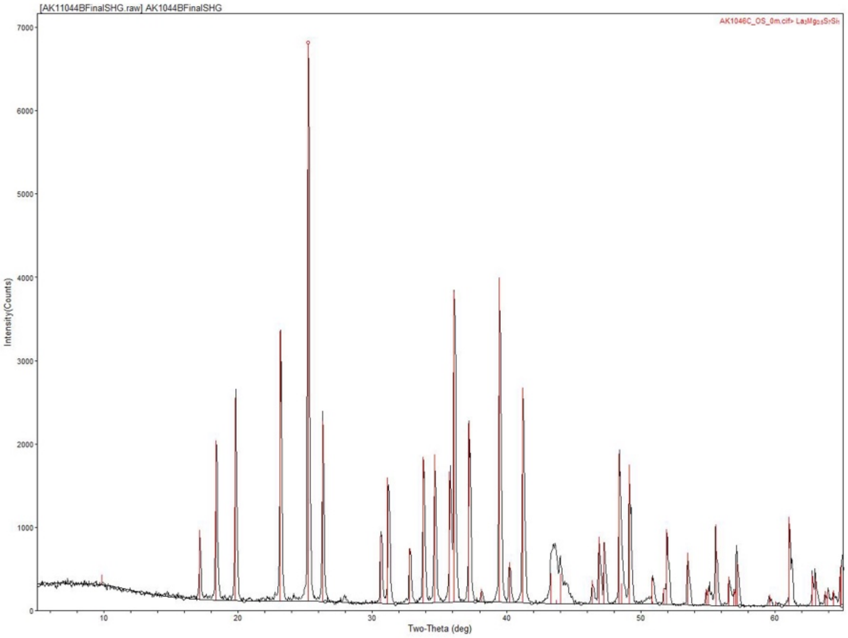

Figure 2.1 Powder X-ray diffraction pattern for $La_3Mg_{0.5}SiS_7$ used for SHG measurement. Data are shown in black and peak positions calculated using the single crystal cif file are shown in red.

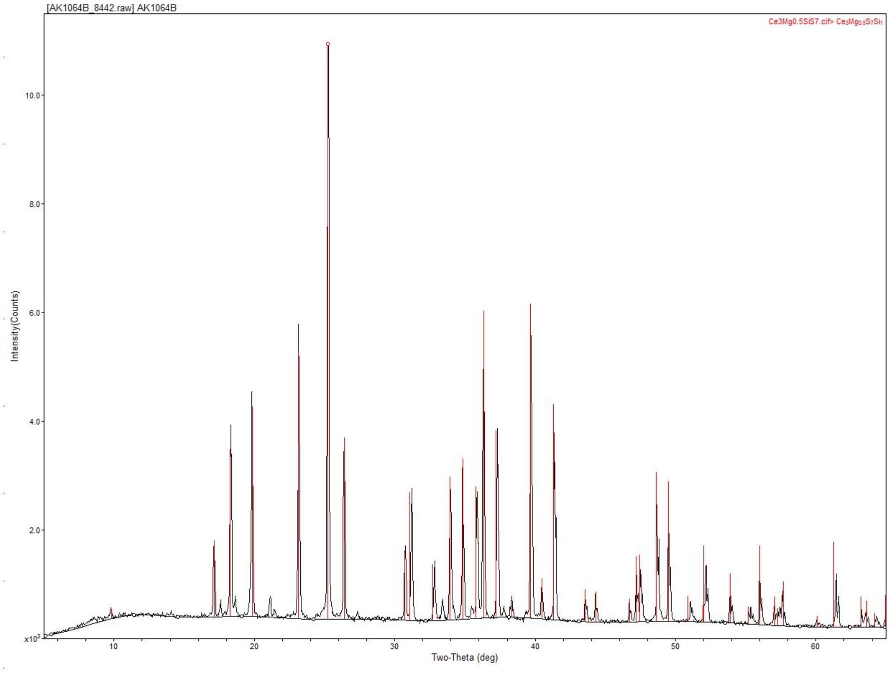

Figure 2.2 Powder X-ray diffraction pattern for $Ce_3Mg_{0.5}SiS_7$ used for magnetic measurements. Data are shown in black and peak positions calculated using the single crystal cif file are shown in red.

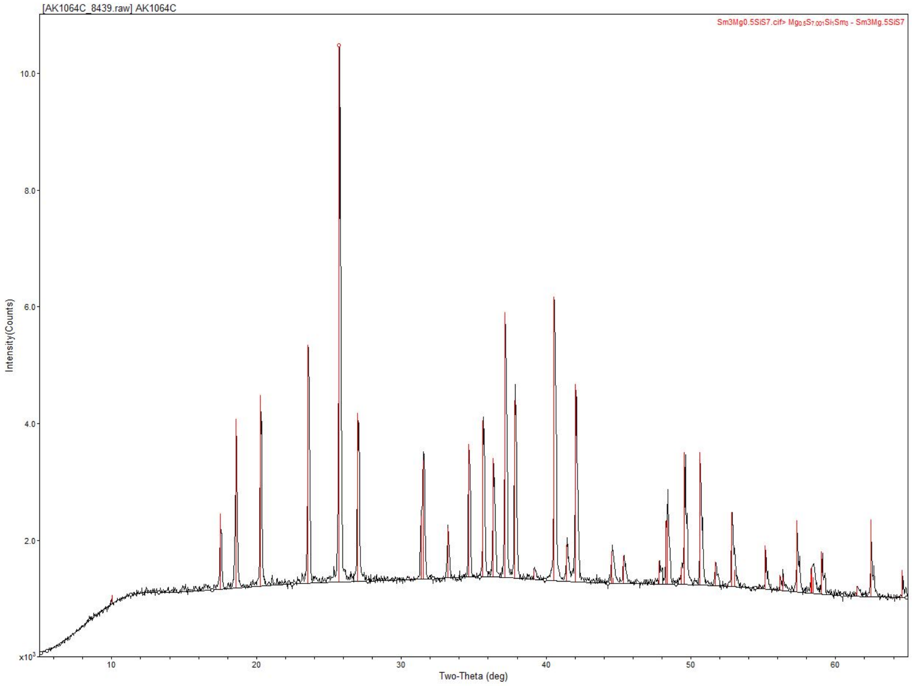

Figure 2.3 Powder X-ray diffraction pattern for $Sm_3Mg_{0.5}SiS_7$ used for magnetic measurements. Data are shown in black and peak positions calculated using the single crystal cif file are shown in red.

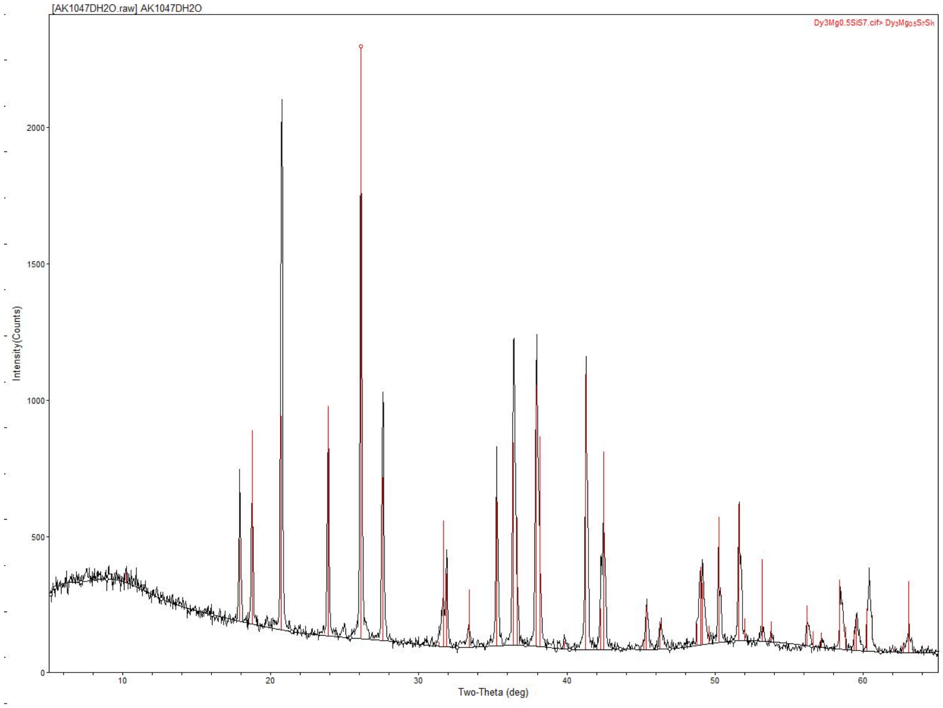

Figure 2.4 Powder X-ray diffraction pattern for $Dy_3Mg_{0.5}SiS_7$ used for magnetic measurements. Data are shown in black and peak positions calculated using the single crystal cif file are shown in red.

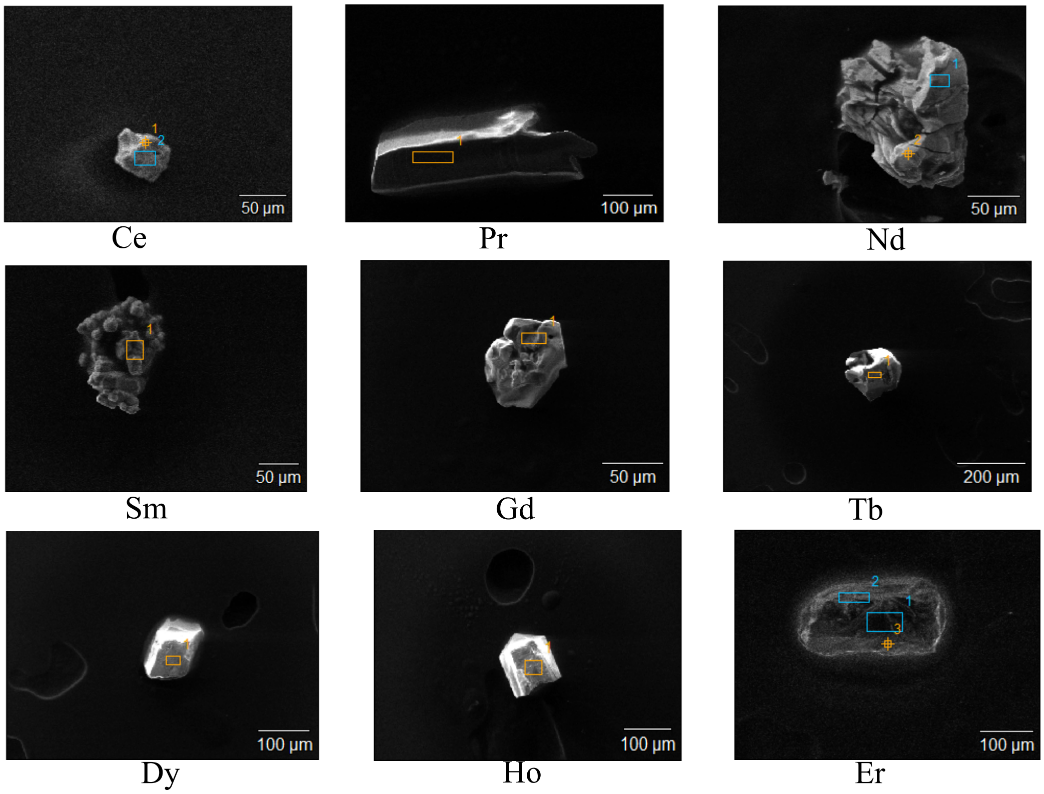

Ce Pr Nd

Sm Gd Tb

Dy Ho Er

Figure 2.5 SEM images of representative crystals of the new thiosilicates synthesized.

Table 2.2 Qualitative Elemental analysis results by EDS

$Ce_3Mg_{0.5}SiS_7$		$Pr_3Mg_{0.5}SiS_7$		$Nd_3Mg_{0.5}SiS_7$		$Sm_3Mg_{0.5}SiS_7$	
Element	Atom %	Element	Atom %	Element	Atom %	Element	Atom %
Ce	24.21	Pr	19.12	Nd	20.77	Sm	26.70
Mg	4.23	Mg	5.82	Mg	4.44	Mg	3.50
Si	8.41	Si	10.83	Si	10.63	Si	11.84
S	63.15	S	64.23	S	64.16	S	57.95

$Gd_3Mg_{0.5}SiS_7$		$Tb_3Mg_{0.5}SiS_7$		$Dy_3Mg_{0.5}SiS_7$		$Ho_3Mg_{0.5}SiS_7$		$Er_3Mg_{0.5}SiS_7$	
Element	Atom %	Element	Atom %	Element	Atom %	Element	Atom %	Element	Atom %
Gd	23.45	Tb	13.07	Dy	18.02	Ho	16.06	Er	15.29
Mg	5.18	Mg	5.15	Mg	5.04	Mg	5.29	Mg	5.21
Si	9.35	Si	12.02	Si	11.41	Si	10.85	Si	10.65
S	62.04	S	69.76	S	65.53	S	67.80	S	68.85

Magnetic Susceptibility

Magnetic property measurements for $Ce_3Mg_{0.5}SiS_7$, $Sm_3Mg_{0.5}SiS_7$, and $Dy_3Mg_{0.5}SiS_7$ were performed using a Quantum Design magnetic property measurement system (QD MPMS 3 SQUID Magnetometer). The magnetic susceptibility was measured under zero-field-cooled (zfc) and field-cooled (fc) conditions from 2 to 300 K in an applied magnetic field of 0.1 T. Magnetization as a function of applied field was measured from −5 to 5 T at 2 K. Data were corrected for the sample shape and radial offset effects as described previously.[30]

UV–Vis Diffuse Reflectance Spectroscopy

UV-vis diffuse reflectance spectroscopy data for $La_3Mg_{0.5}SiS_7$ was obtained using a PerkinElmer Lambda 35 UV-vis scanning spectrophotometer equipped with an integrating sphere in range 300-900 nm. The reflectance data was then converted to absorbance data using the Kubelka-Munk function.[31]

Second Harmonic Generation (SHG)

The Kurtz−Perry method was adopted to assess the SHG performance of the sample. Polycrystalline powder of the sample was placed in the tubes of quartz, and then were irradiated with a pulsed infrared beam (1064 nm) produced by a Q-switched Nd: YAG laser. The generated second harmonic signals (532 nm） were collected by the detector. KDP (KH_2PO_4) served as a standard during the SHG test procedure.[32, 33]

Results and Discussion

Synthesis

A review of $RE_3M_{0.5}MQ_7$ (M=Metal) compounds reveals that a significant number of compositions that are structurally and compositionally related to $RE_3M_{0.5}MQ_7$ have not been reported. To explore some of these compositions and to extend the use of our BCM method to more diverse structural families, we decided to synthesize the $RE_3Mg_{0.5}SiS_7$ family both as powders and as single crystals using the BCM method. Table 2.3 list the known compositions of the $RE_3Mg_{0.5}SiS_7$ structure type, while table 2.4 lists the known compositions of the $RE_3Mg_{0.5}GeS_7$ structure type done prior to this work; clearly more thiogermanates than thiosilicates have been reported.[20] We performed the synthesis of the $RE_3Mg_{0.5}SiS_7$ RE = La, Ce, Pr, Nd, Sm-Er series, targeting both single crystals and powders. Using NaI (Nd, Sm-Er) and $CaCl_2$/NaCl (La, Ce, Pr) as fluxes and using boron powder to remove the oxygen from our RE_2O_3 reagents, we successfully obtained high quality single crystals for all the target compositions. Although the RE = Sm-Er target phases were crystallized as the major product, $Mg_2(SiS_4)$ was identified as a minor impurity phase in these reactions and, even after numerous attempts to optimize the flux crystal growth reaction conditions, could not be eliminated. For RE = La-Nd the target phases would not form when using the same synthetic procedure used to obtain the RE=Sm-Er compounds due to the formation of $RE_3(SiS_4)_2I$ as the major reaction product.[34] It is important to note that while $Sm_3(SiS_4)_2I$ has been reported, the chlorine analog has not.[35] This may be the reason the NaI flux was able to be used to successfully synthesize the target samarium analog. To eliminate the $RE_3(SiS_4)_2I$ phases entirely from the product the NaI flux was changed to the NaCl/$CaCl_2$ eutectic. This led to the successful synthesis of the target phases, $La_3Mg_{0.5}SiS_7$ and $Pr_3Mg_{0.5}SiS_7$, which formed as minor products along with a new rare earth calcium containing thiosilicate as the major product. We will report on the latter materials in the near future. To eliminate the formation of this calcium containing phase for the synthesis of the cerium and neodymium phases, a NaCl flux was used. The target phase, $Ce_3Mg_{0.5}SiS_7$, was successfully synthesized using this method. The target phase, $Nd_3Mg_{0.5}SiS_7$, was synthesized by decreasing the flux amount from 200 mg to 75 mg. Attempts at the synthesis of RE = Tm-Lu using the synthetic routes described above failed. In all cases only $MgRE_2S_4$ and $Mg_2(SiS_4)$ were isolated. This is perhaps not unexpected as no other RE-Mg-Si-S compositions belonging to this structure type have been reported, as illustrated by table 2.3.

The post reaction workup of all targeted material was initially preformed using methanol, however impurities remained. For that reason, water was used for the workup after discovering the target compositions are reasonably air and water stable.

Table 2.3 Known thiosilicate compounds of the $Ln_3Mg_{0.5}SiS_7$ structure type

Ln^{3+} M^{2+}	La	Ce	Pr	Nd	Sm	Gd	Tb	Dy	Ho	Er	Ref
Mg	•										23, 24
Cr	•										22, 23
Mn	•	•	•	•	•	•		•		•	9, 22, 23
Fe	•				•						23, 18, 22
Co	•										15, 22
Ni	•										15, 22
Zn	•	•	•	•	•	•	•	•	•	•	20
Cd	•	•	•	•	•	•	•	•	•		20

•-Reported compound

Table 2.4 Known thiogermanate compounds of the $Ln_3Mg_{0.5}GeS_7$ structure type

Ln^{3+} M^{2+}	La	Ce	Pr	Nd	Sm	Gd	Tb	Dy	Ho	Er	Ref
Mg	•	•	•	•	•	•	•	•	•	•	24, 13
Cr	•										23
Mn	•	•	•	•	•	•	•	•	•	•	11, 23
Fe	•	•	•	•	•	•	•	•	•	•	10
Co	•	•	•	•	•	•	•	•	•	•	12, 14
Ni	•	•	•	•	•	•	•	•	•	•	12, 14
Zn	•	•	•	•	•	•	•	•	•	•	20
Cd	•	•	•	•	•	•	•	•			20

•-Reported compounds

Structure Description

The $RE_3Mg_{0.5}SiS_7$ structure is a member of the $RE_3M_{0.5}MQ_7$ family of compounds that crystallizes in the hexagonal crystal system, adopting the noncentrosymmetric space group, $P6_3$. All of the title compositions are isostructural and crystallize in this space group. This three-dimensional structure is made up of RES_8 bi-capped trigonal prisms that edge and corner share to create a ring-like structure. Isolated SiS_4 tetrahedra throughout the structure are located between each ring-like structure of RES_8 bi-capped trigonal prisms. Face sharing MgS_6 octahedra tunnel through the middle of the ring-like structure. Figure 2.6 illustrates the local coordination environments of the RE^{+3}, Si^{+4}, and Mg^{+2} cations respectively, along with the general structure of $RE_3Mg_{0.5}SiS_7$. Figure 2.7 contains a plot of the unit cell volume of $RE_3Mg_{0.5}SiS_7$ as a function of the rare-earth ionic radius. The decrease in volume when going from La to Er is expected due to the lanthanide contraction in these compounds.

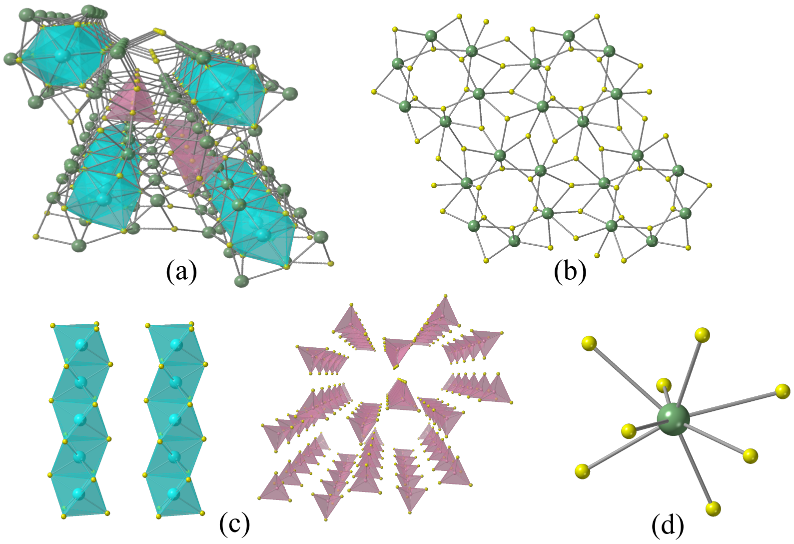

Figure 2.6 (a) 3D framework structure of $Gd_3Mg_{0.5}SiS_7$ viewed down the c-direction (b) GdS_8 chains developing the framework (c) face-sharing MgS_6 octahedra and isolated SiS_4

tetrahedra (d) Gd coordination environment.

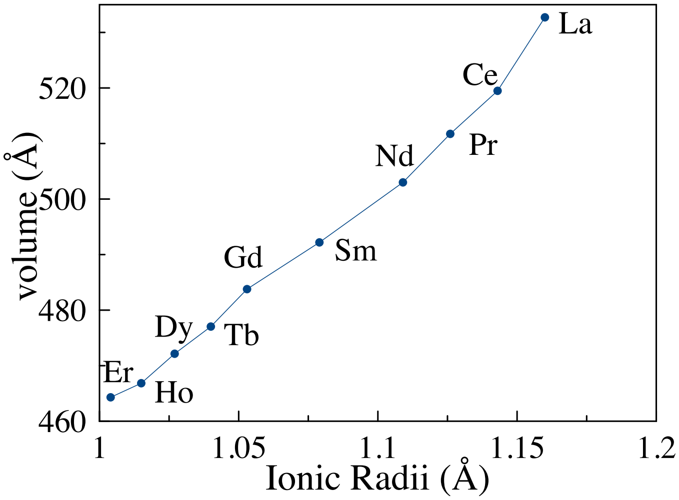

Figure 2.7 Volume vs ionic radii of the RE^{3+} elements in the $RE_3Mg_{0.5}SiS_7$ structure.

Magnetic Properties

The magnetic susceptibility data for $Ce_3Mg_{0.5}SiS_7$, $Dy_3Mg_{0.5}SiS_7$, and $Sm_3Mg_{0.5}SiS_7$ are shown in figure . The data in these plots were analyzed and the magnetic moment extracted from a fit to the Curie Weiss Law. The moments and Weiss constants are summarized in table 2.5 and were found to be in excellent agreement with the calculated moments. The negative Weiss temperatures suggest antiferromagnetic interactions, but as seen in figure 2.8, no antiferromagnetic transitions are observed above 2 K, the lowest temperature measured.

Table 2.5 Magnetic data for $Ce_3Mg_{0.5}SiS_7$, $Dy_3Mg_{0.5}SiS_7$

Compound	Observed μ_{eff} (μ_B/Ln^{3+}) from Curie–Weiss fit (200–300 K)	calculated μ_{eff} (μ_B/Ln^{3+})	Θ_W (K)
$Ce_3Mg_{0.5}SiS_7$	2.33	2.54	-43.7
$Dy_3Mg_{0.5}SiS_7$	10.67	10.65	-5.4

The samarium analog, as expected, exhibits Van Vleck Paramagnetism in the 2-300 K temperature range measured.[36] Due to the lack of Curie-Weiss behavior the effective moment of Sm^{3+} at room temperature was determined to be 1.45 μ_B/Sm^{3+}. This is in agreement with other Sm chalcogenides such as the reported $BaSm_2S_4$, which has an experimentally reported moment of 1.47 μ_B/Sm^{3+}.[37]

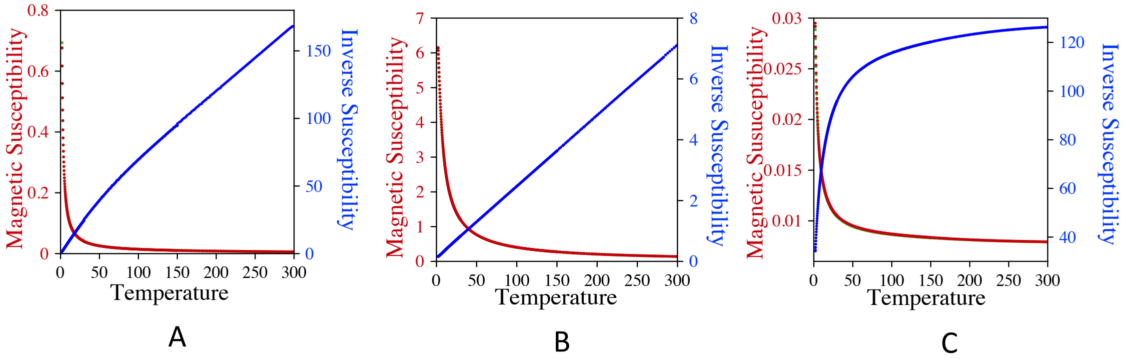

Figure 2.8 Molar and Inverse Susceptibility vs Temperature for $Ce_3Mg_{0.5}SiS_7$ (A), $Dy_3Mg_{0.5}SiS_7$ (B), and $Sm_3Mg_{0.5}SiS_7$ (C)

Optical Properties

UV-vis diffuse reflectance spectroscopy was performed on $La_3Mg_{0.5}SiS_7$ and it was determined that the compound is a direct band gap semiconductor with a band gap of 2.77 eV (Fig. 2.9). Materials that crystallize in a noncentrosymmetric crystal class may exhibit SHG behavior.[36] A multitude of reported $RE_3M_{0x}MQ_7$ have had their SHG properties analyzed.[38, 39] La_3LiMS_7 (M= Ge, Sn) exhibits a strong NLO effect and high laser damage threshold (LDT). Likely caused by a mixed contribution of LnS_8 and MS_4 ligands.[40] Due to this, we decided to investigate the SHG properties of one of the title compounds $La_3Mg_{0.5}SiS_7$. $La_3Mg_{0.5}SiS_7$ was determined to be SHG-active with an efficiency of ~0.16 times the standard potassium dihydrogen phosphate (KDP). Figure 4 shows the SHG intensity vs time of $La_3Mg_{0.5}SiS_7$ and the KDP standard. Due to the coloration of the crystals of the other compositions that interferes with SHG measurements, no other samples were tested for SHG activity.

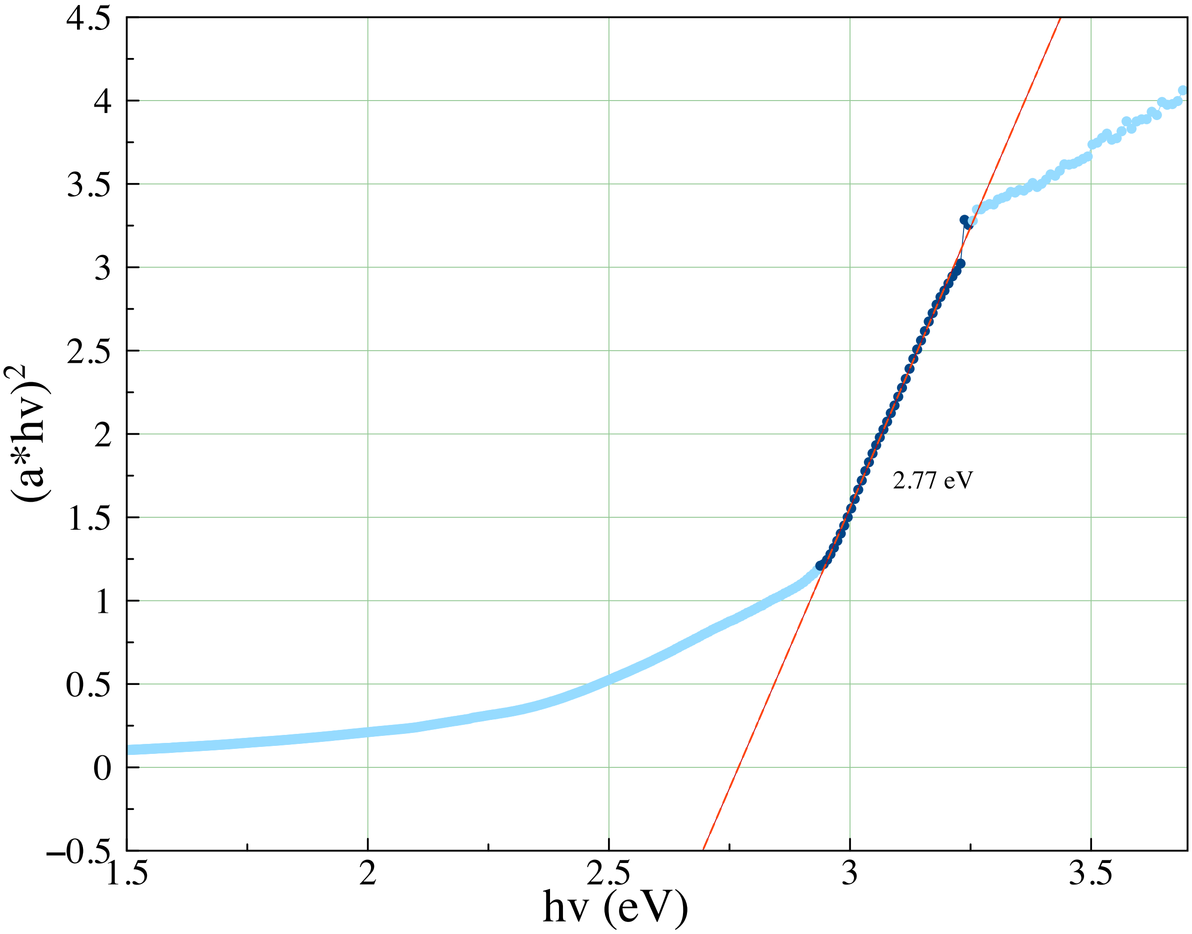

Figure 2.9 Tauc plot for select compositions for $La_3Mg_{0.5}SiS_7$ plotted as direct band gap materials.

Conclusion

In this paper, we report the successfully preparation of nine new members of the $RE_3Mg_{0.5}SiS_7$ series, $RE_3Mg_{0.5}SiS_7$ (RE=La-Nd, Sm-Er), representing an addition to the larger $RE_3M_{1-x}M_xQ_7$ family of compounds. By combining the BCM method and molten flux growth, we succeeded in preparing high-quality single crystals of $RE_3Mg_{0.5}SiS_7$ (RE=La-Nd, Sm-Er) using binary oxides as starting reagents. In addition, we combined the BCM method with solid state synthesis to prepare phase pure polycrystalline powders for property measurements. Due to the non-centrosymmetry of the crystal structure, SHG behavior of $La_3Mg_{0.5}SiS_7$ compound was measured showing that this compound is SHG active with an intensity of 0.16 x KDP. $Ce_3Mg_{0.5}SiS_7$, $Dy_3Mg_{0.5}SiS_7$, and $Sm_3Mg_{0.5}SiS_7$, exhibit paramagnetic behavior with no obvious magnetic ordering down to 2 K.

The BCM method is a valuable tool in metal chalcogenide synthesis as it provided more facile access to compounds due to the use of commercially readily available oxide reagents and can be used to synthesize a wide variety of new compositions in single crystal form. As the BCM method is still relatively new, we are in the process of expanding the BCM method to related thiosilicate compositions in order to explore their physical properties.

ACKNOWLEDGMENTS: Research supported by the US Department of Energy, Office of Basic Energy Sciences, Division of Materials Sciences and Engineering under award DE-SC0018739. Synthesis, structural characterization, and magnetic studies performed at UofSC. SHG measurements performed at the University of Houston, supported by NSF DMR-2002319.

References

1. Kanatzidis, M. G. Discovery-Synthesis, Design, and Prediction of Chalcogenide Phases. *Inorg. Chem.* ***2017,*** *56, 3158-3173.*
2. Breton, L. S.; Smith, M. D.; zur Loye, H.-C. Trends in Rare Earth Thiophosphate Syntheses: $Rb_3Ln(PS_4)_2$ (Ln = La, Ce, Pr), $Rb_{3-x}Na_xLn(PS_4)_2$ (Ln = Ce, Pr; $x = 0.50$, 0.55), and $RbEuPS_4$Obtained by Molten Flux Crystal Growth. *CrystEngComm.* ***2021,*** *23, 5241-5248.*
3. Usman, M.; Smith, M. D.; Morrison, G.; Klepov, V. V.; Zhang, W.; Halasyamani, P. S.; zur Loye, H.-C. Molten Alkali Halide Flux Growth of an Extensive Family of Noncentrosymmetric Rare Earth Sulfides: Structure and Magnetic and Optical (SHG) Properties. *Inorg. Chem.* ***2019,*** *58, 8541-8550.*
4. Breton, L. S.; Morrison, G.; Lacroix, M. R.; Halasyamani, P. S.; zur Loye, H.-C. Lanthanide thioborates, an emerging class of nonlinear optical materials, efficiently synthesized using the boron-chalcogen mixture method. *Chem. Commun.(Camb).* ***2022,*** *58, 7992-7995.*
5. Breton, L. S.; Klepov, V. V.; zur Loye, H.-C. Facile Oxide to Chalcogenide Conversion for Actinides Using the Boron-Chalcogen Mixture Method. *J Am. Chem. Soc.* ***2020,*** *142, 14365-14373.*
6. Wu, L.-M.; Seo, D. K. New solid-gas metathetical synthesis of binary metal polysulfides and sulfides at intermediate temperatures: utilization of boron sulfides. *J. Am. Chem. Soc.* ***2004,*** *126, 4676-4681.*
7. Huang, Y.-Z.; Chen, L.; Wu, L.-M. Crystalline Nanowires of Ln_2O_2S, $Ln_2O_2S_2$, LnS_2 (Ln = La, Nd), and $La_2O_2S:Eu^{3+}$. Conversions via the Boron-Sulfur Method That Preserve Shape. *Cryst. Growth Des.* ***2008,*** *8, 739-743.*
8. Huang, Y.-Z.; Chen, L.; Wu, L.-M. Submicrosized rods, cables, and tubes of ZnE (E = S, Se, Te): exterior-interior boron-chalcogen conversions and optical properties. *Inorg. Chem.* ***2008,*** *47, 10723-10728.*
9. Collin G.; Laurelle, P. Structure de $La_6Cu_2Si_2S_{14}$. *Bull. Soc. Fr. Mineral. Cristallogr.* ***1971,*** *94, 175-176.*
10. Daszkiewicz, M.; Pashynska, Y. O.; Marchuk, O. V.; Gulay, L. D.; Kaczorowski, D. Crystal structure and magnetic properties of $R_3Fe_{0.5}GeS_7$ (R = Y, La, Ce, Pr, Sm, Gd, Tb, Dy, Ho, Er and Tm). *J. Alloys Compd.* ***2014,*** *616, 243-249.*
11. Daszkiewicz, M.; Marchuk, O. V.; Gulay, L. D.; Kaczorowski, D. Crystal structure and magnetic properties of $R_3Mn_{0.5}GeS_7$ (R=Y, Ce, Pr, Nd, Sm, Gd, Tb, Dy, Ho and Er). *J. Alloys Compd.* ***2014,*** *610, 258-263.*
12. Daszkiewicz, M.; Pashynska, Y. O.; Marchuk, O. V.; Gulay, L. D.; Kaczorowski, D. Crystal structure and magnetic properties of $R_3Co_{0.5}GeS_7$ (R = Y, La, Ce, Pr, Nd, Sm, Gd, Tb, Dy, Ho, Er and Tm) and $R_3Ni_{0.5}GeS_7$(R = Y, Ce, Sm, Gd, Tb, Dy, Ho, Er and Tm). *J Alloys Compd.* ***2015,*** *647, 445-455.*
13. Huch, M. R.; Gulay, L. D.; Olekseyuk, I. D. Crystal structures of the $R_3Mg_{0.5}GeS_7$ (R=Y, Ce, Pr, Nd, Sm, Gd, Tb, Dy, Ho and Er) compounds. *J Alloys Compd.* ***2006,*** *424, 114-118.*
14. Iyer, A. K.; Yin, W.; Lee, E. J.; Lin, X.; Mar, A.; Lin, X.; Mar, A. Quaternary rare-earth sulfides $RE_3M_{0.5}GeS_7$ (RE=La–Nd, Sm; M=Co, Ni) and $Y_3Pd_{0.5}SiS_7$. *J. Solid State Chem.* ***2017,*** *250, 14-23.*

15. Jin, Z.; Li, Z.; Du, Y. Synthesis and the crystal structure of $La_6NiSi_2S_{14}$ and $La_6CoSi_2S_{14}$. *Yingyong Huaxue.* ***1985,*** *2, 42-46.*
16. Michelet, A.; Flahaut, J. Sur les composés du type $La_6MnSi_2S_{14}$. *C. R. Acad. Sci. Ser. C.* ***1969,*** *269 , 1203-1205.*
17. Strok, O.; Daszkiewicz, M.; Gulay, L. Crystal structure of $R_3Mg_{0.5}DSe_7$ (R = Ce, Pr; D = Si, Ge). *Chem. Met. Alloys.* ***2015,*** *8, 16-21.*
18. Sun, Y.-L.; Yang, C.; Guo, S.-P. Synthesis and crystal structure of a new quaternary sulfide $FeSm_6Si_2S_{14}$. *Jiegou Huaxue.* ***2013,*** *202, 269-275.*
19. Yin, W.; Wang, W.; Kang, L.; Lin, Z.; Feng, K.; Shi, Y.; Hao, W.; Yao, J.; Wu, Y. Ln_3FeGaQ_7: A new series of transition-metal rare-earth chalcogenides. *J. Solid State Chem.* ***2013,*** *202, 269-275.*
20. Zhou, Y.; Iyer, A. K.; Oliynyk, A. O.; Heyberger, M.; Lin, Y.; Qiu, Y.; Mar, A. O.-H. Quaternary rare-earth sulfides $RE_3M_{0.5}M'S_7$ (M = Zn, Cd; M′ = Si, Ge). *J. Solid State Chem.* ***2019,*** *278, 120914.*
21. Wu, L.-B.; Huang, F.-Q. Crystal structure of trilanthanum monosilver monosilicon heptasulfide, La_3AgSiS_7. *Z. fur Krist. - New Cryst. Struct.* ***2005,*** *220, 327-328.*
22. Akopov, G.; Hewage, N. W.; Yox, P.; Viswanathan, G.; Lee, S. J.; Hulsebosch, L. P.; Cady, S. D.; Paterson, A. L.; Perras, F. A.; Xu, W.; Wu, K.; Mudryk, Y.; Kovnir, K. Synthesis-enabled exploration of chiral and polar multivalent quaternary sulfides. *Chem. Sci. J.* ***2021,*** *12, 14718-14730.*
23. Collin, G.; Laurelle, P. Structure cristalline de $La_6MnSi_2S_{14}$. *C. R. Acad. Sci. Ser. C.* ***1970,*** *270, 410-412.*
24. Gitzendanner, R. L.; Spencer, C. M.; DiSalvo, F. J.; Pell, M. A.; Ibers, J. A. Synthesis and Structure of a New Quaternary Rare-Earth Sulfide, $La_6MgGe_2S_{14}$, and the Related Compound $La_6MgSi_2S_{14}$. *J. Solid State Chem.* ***1997,*** *131, 399-404.*
25. Lin, F.; Luo, M.; Wang, R.; Che, X.; Huang, F. $La_6Cd_{0.75}Ga_2Q_{11.5}Cl_{2.5}$ (Q = S and Se): two new nonlinear optical chalcohalides with a large laser-induced damage threshold. *CrystEngComm.* ***2021,*** *23, 2133-2137.*
26. He, J.; Wang, Z.; Zhang, X.; Cheng, Y.; Gong, Y.; Lai, X.; Zheng, C.; Lin, J.; Huang, F. Synthesis, structure, magnetic and photoelectric properties of $Ln_3M_{0.5}M'Se_7$ (Ln = La, Ce, Sm; M = Fe, Mn; M′ = Si, Ge) and $La_3MnGaSe_7$. *RSC Advances.* ***2015,*** *5, 52629-52635.*
27. Krause, L.; Herbst-Irmer, R.; Sheldrick, G. M.; Stalke, D. Comparison of silver and molybdenum microfocus X-ray sources for single-crystal structure determination. *J. Appl. Crystallogr.* ***2015,*** *48, 3-10.*
28. Sheldrick, G. M. *Shelxt*– Integrated Space-Group and Crystal-Structure Determination. *Acta Crystallogr. A.* ***2015,*** *71, 3-8.*
29. Hübschle, C. B.; Sheldrick, G. M.; Dittrich, B. ShelXle: a Qt graphical user interface for SHELXL. *J Appl. Crystallogr.* ***2011,*** *44, 1281-1284.*
30. Morrison, G.; zur Loye, H.-C. Simple Correction for the Sample Shape and Radial Offset Effects on SQUID Magnetometers: Magnetic Measurements on Ln_2O_3(Ln=Gd, Dy, Er) Standards. *J. Solid State Chem.* ***2015,*** *221, 334-337.*
31. Kubelka, P.; Munk, F. F. Ein Beittrag zur Optik der Farbanstriche. *Z. Technol. Phys.* ***1931,*** *593.*
32. Kurtz, S. K.; Perry, T. T. A Powder Technique for the Evaluation of Nonlinear Optical Materials. *J. Appl. Phys.* ***1968,*** *39, 3798-3813.*

33. Ok, K. M.; Chi, E. O.; Halasyamani, P. S. Bulk characterization methods for non-centrosymmetric materials: second-harmonic generation, piezoelectricity, pyroelectricity, and ferroelectricity. *Chem. Soc. Rev.* ***2006,*** *35, 710-717.*
34. Hatscher, S. T. U., W. Synthese Und Kristallstrukturen Von $Ln_3I(SiS_4)_2$ (LN=Pr, Nd, Sm, Tb). *Z. anorg. allg. Chem.* ***2001,*** *627, 2198.*
35. Hatscher, S. T.; Urland, W. Synthesis and structures of chloride thiosilicates with lanthanides $Ln_3Cl[SiS_4]_2$ (Ln = La, Ce, Pr). *Mater. Res. Bull.* ***2002,*** *37, 1239-1247.*
36. Vleck, V.; Hasbrouck, J. The theory of electric and magnetic susceptibilities. *Oxford University Press.* ***1965.***
37. Yoshitaka, M.; Yoshihiro, D.; Yukio, H. Crystal structures and magnetic properties of ternary sulfides $BaLn_2S_4$ (Ln = Sm, Gd-Lu). *J. Ceram. Soc. Japan.* ***2009,*** *117, 85-88.*
38. Shi, Y.-F.; Chen, Y.-k.; Chen, M.-C.; Wu, L.-M.; Lin, H.; Zhou, L.-J.; Chen, L. Strongest Second Harmonic Generation in the Polar R_3MTQ_7Family: Atomic Distribution Induced Nonlinear Optical Cooperation. *Chem. Mater.* ***2015,*** *27, 1876-1884.*
39. Poduska, K. M.; DiSalvo, F. J.; Min, K.; Halasyamani, P. S. Structure determination of La_3CuGeS_7 and $La3_{Cu}GeSe_7$. *J. Alloys Compd.* ***2002,*** *335, L5-L9.*
40. Yang, Y.; Chu, Y.; Zhang, B.; Wu, K.; Pan, S. Unique Unilateral-Chelated Mode-Induced d–p−π Interaction Enhances Second-Harmonic Generation Response in New Ln_3LiMS_7 Family. *Chem. Mater.* ***2021,*** *33, 4225-4230.*

CHAPTER 3:

Magnetic Property Analysis of an Extensive Family of Quaternary Novel Rare Earth Transition Metal Thiosilicates Obtained Via Molten Alkali Halide Flux Growth Combined with the Boron Chalcogen Mixture Method

Abstract:

$RE_3TM_{0.5}SiS_7$ (RE= Gd-Yb, TM= Fe, Co, Ni) a series of transition metal containing thiosilicates exhibiting unique magnetic properties are reported on. The target compounds have been synthesized using a combination of molten alkali halide flux growth and the BCM method. The compounds crystalize in the hexagonal crystal system in the $P6_3$ space group. Herein, we discuss the use of the Boron Chalcogen Mixture (BCM) method to synthesize phase pure samples of the title compounds for magnetic measurements without the difficulties that plague typical chalcogenide synthesize. The compounds are antiferromagnetic featuring a transition between 2-20 K. This is also the first reported Ytterbium containing compounds of this structure type as all other reported series only report on Thulium as the latest rare earth.

Introduction:

The search for new chalcogenide materials continues to be a worthy endeavor as many have shown to have desirable physical properties.[1, 2] One particular class of chalcogens recently shown to have potentials in many of these properties are the chalcometallates.[3, 4] Because of this these metal chalcogenides are starting to be found in multiple areas of cutting-edge research such as fast ion conductors,[5, 6] radiation detectors,[7-9] nonlinear optics,[10-12] and novel magnetic materials, to name a few.[13, 14] Recently, we have reported on the thiosilicates, a class of chalcometallates, of chemical formula $RE_3Mg_{0.5}SiS_7$ to form readily using a combination of the BCM and molten flux methods.[15] In this paper, we emphasize the lack of thiosilicates in this $RE_3M_xMS_7$ family, showing a large compositional phase space still empty.[16] Recent research has shown the ability to incorporate transition metals into this phase.[17-25] Specifically, Akopov et al show the synthesis and characterization of $La_3TM_xSiS_7$ (TM= Transition Metals). To continue our research on these compounds and build upon theirs, we wanted to analyze the later rare earth elements in this phase focusing on having two magnetic sublattices as Lanthanum is nonmagnetic.

With the inclusion of transition metals, these $RE_3M_xMS_7$ phases have shown unique magnetism and potentials in optical properties. For example, $La_6Cu_2Si_2S_{14}$ exhibits not only phase match ability but also second harmonic generation (SHG) values comparable to the standard $AgGaS_2$, while $RE_3Fe_{0.5}GeS_7$ (Re=Gd, Tb, Dy, Ho, Er and Tm) show antiferromagnetic ordering at low temperatures.[17, 25] However, the thiosilicate phases have only had magnetic properties reported on for the non-magnetic rare earth Lanthanum. As previously stated, with the addition of a magnetic rare earth such as terbium, the magnetic properties become much more unique, due to the presence of two magnetic sublattices. Herein, we report on the synthesis of high-quality single crystals, of $RE_3TM_{0.5}SiS_7$ (RE=Gd-Yb) TM=(Fe, Co, Ni) for their structural determination and magnetic property measurements.

Experimental

RE_2O_3 (RE= Gd, Dy, Ho, Er, Tm, Yb) (99.9%, Alfa Aesar), Tb_4O_7 (99.9% Alfa Aesar), Sulfur (Fischer Scientific), Boron (99.9%, Beantown Chemical) , SiO_2 (99.9%, Alfa Aesar), NaI (99.9%, Beantown Chemical) Fe_2O_3, Nickel, and Cobalt powder reagents were used to synthesize the target compounds. NaI was stored in a drying oven set to 260°C due to its hydroscopic nature. $RE_3TM_{0.5}SiS_7$ title compounds were synthesized by the RE_2O_3 , Boron, Sulfur, SiO_2 , and TM/Fe_2O_3 powders in a 3:20:30:2:1 molar ratio (0.5 for Fe_2O_3) , respectively, into a fused silica tube (10 x 12 mm inner and outer diameters, about 150 mm length) along with 250 mg of NaI flux. The fused silica tube was evacuated to 10^{-4} torr and flame sealed using a methane/oxygen torch. The sealed fused silica tube was placed into a programmable furnace set to heat to 850°C in 20 hours, to dwell at this temperature for 20 hours, and to cool to 550°C in 20 hours, at which point the furnace was shut off and allowed to return to room temperature. After reactions finished, methanol and water were used for the dissolution of the flux and impurities in the product.

Single-Crystal X-ray Diffraction (SXRD):

X-ray intensity data of black plate crystals of all title compositions were collected at 300 K using a Bruker D8 QUEST diffractometer equipped with a PHOTON-II area detector and an Incoatec microfocus source (Mo Kα radiation, $\lambda = 0.71073$ Å). Single crystals were mounted on a microloop with immersion oil. The raw area detector data frames were reduced and corrected for absorption effects using the SAINT+ and SADABS programs.[26] Final unit cell parameters were determined by the least-squares refinement of a large array of reflections form each data set.[27] An initial structural model was obtained with SHELXT. Subsequent difference Fourier calculations and full-matrix least-squares refinement against F2 were performed with SHELXL-2018 using the ShelXle interface.[28] All compounds crystalize in the noncentrosymmetric, hexagonal space group $P6_3$, which is uniquely confirmed by the pattern of systematic absences in the intensity data. The asymmetric unit contains one rare earth atom, one transition metal atom, one silicon atom, and three sulfur atoms. All atoms are all located on positions of general crystallographic symmetry. All atoms were refined with anisotropic displacement parameters. The crystallographic data and diffraction results are listed in table 3.1.

Table 3.1 Crystallographic Data and diffraction results for all reported compounds

Chemical formula	$Gd_3Fe_{0.5}SiS_7$	$Gd_3Co_{0.5}SiS_7$	$Gd_3Ni_{0.5}SiS_7$	$Tb_3Fe_{0.5}SiS_7$	$Tb_3Co_{0.5}SiS_7$
Formula weight		753.72	753.60	757.20	788.77
Crystal system	Hexagonal				
Space group, Z	$P6_3$	$P6_3$	$P6_3$	$P6_3$	$P6_3$
a, Å	10.35010(10)	9.8937(3)	9.9231(6)	9.8539(11)	9.6400(3)
c, Å	5.74220(10)	5.6521(3)	5.6470(5)	5.6456(9)	5.6838(2)
V, Å^3	532.719	479.13(4)	481.55(7)	474.74(13)	457.43(3)
ρ_{calcd}, g/cm^3	4.248	2.612	5.197	5.297	5.727
Radiation (λ, Å)	Mo-Kα (0.710173 Å)				
μ, mm^{-1}	13.259	11.466	22.934	24.426	31.366
T, K	399.12	298.64	297.69	297.09	299.34
Crystal dim., mm^3	0.04 x 0.04 x 0.04	0.05 x 0.03 x 0.03	0.04 x 0.04 x 0.04	0.05 x 0.05 x 0.05	0.05 x 0.05 x 0.05
2θ range, deg.	3.938-36.302	2.377-36.298	42.370-36.331	2.387-36.303	2.344-36.341
Reflections collected	22794	20451	20689	20320	19190
Data/parameters/restraints	1737/38/1	1546/38/1	1564/38/1	1529/38/1	1478/39/1
R_{int}	0.0280	0.0313	0.0320	0.0325	0.0314
Goodness of fit	1.165	1.221	1.188	1.252	1.297
$R_1(I > 2\sigma(I))$	0.0077	0.0112	0.0097	0.0093	0.0159
wR_2 (all data)	0.0179	0.0260	0.0204	0.0215	0.0408

Chemical formula	$Tb_3Ni_{0.5}SiS_7$	$Dy_3Fe_{0.5}SiS_7$	$Dy_3Co_{0.5}SiS_7$	$Dy_3Ni_{0.5}SiS_7$	$Ho_3Fe_{0.5}SiS_7$
Formula weight	758.70	767.93	769.48	769.44	775.22
Crystal system	Hexagonal				
Space group, Z	$P6_3$	$P6_3$	$P6_3$	$P6_3$	$P6_3$
a, Å	9.82720(10)	9.7645(2)	9.8120(5)	9.77530(10)	9.7556(6)
c, Å	5.63800(10)	5.6837(2)	5.6930(4)	5.63770(10)	5.6445(5)
V, Å^3	471.536(13)	469.31(3)	474.70(6)	466.544(13)	465.23(7)
ρ_{calcd}, g/cm^3	5.343	5.434	5.383	5.477	2.767
Radiation (λ, Å)	Mo-Kα (0.710173 Å)				
μ, mm^{-1}	24.821	25.987	25.799	26.372	13.817
T, K	297.05	297.38	297.43	297.69	298.11
Crystal dim., mm^3	0.06 x 0.05 x 0.05	0.05 x 0.05 x 0.05	0.05 x 0.05 x 0.05	0.05 x 0.05 x 0.05	0.04 x 0.04 x 0.04
2θ range, deg.	2.393-36.310	2.408-36.357	2.397-36.152	2.406-36.319	2.411-36.315
Reflections collected	19617	19831	9087	20130	19819
Data/parameters/restraints	1511/38/1	1516/39/1	1461/38/1	1513/38/1	1507/38/1
R_{int}	0.0372	0.0312	0.0369	0.0314	0.0319
Goodness of fit	1.366	1.183	1.112	1.184	1.225
$R_1(I > 2\sigma(I))$	0.0135	0.0218	0.0223	0.094	0.0097
wR_2 (all data)	0.0320	0.0521	0.0426	0.0194	0.0229

Chemical formula	$Ho_3Co_{0.5}SiS_7$	$Ho_3Ni_{0.5}SiS_7$	$Er_3Fe_{0.5}SiS_7$	$Er_3Co_{0.5}SiS_7$	$Er_3Ni_{0.5}SiS_7$
Formula weight	776.84	776.66	782.21	783.76	783.72
Crystal system	Hexagonal				
Space group, Z	$P6_3$	$P6_3$	$P6_3$	$P6_3$	$P6_3$
a, Å	9.73990(10)	9.73310(10)	9.7107010)	9.6948(3)	9.68260(10)
c, Å	5.65100(10)	5.64320(10)	5.65080(10)	5.6667(3)	5.65190(10)
V, Å^3	464.264(13)	462.976(6)	461.468(13)	461.25(4)	458.890 (12)
ρ_{calcd}, g/cm^3	5.557	2.786	2.815	5.643	5.671
Radiation (λ, Å)	Mo-Kα (0.710173 Å)				
μ, mm^{-1}	27.803	14.001	214.709	29.545	29.819
T, K	299.19	298.96	297.67	297.73	297.93
Crystal dim., mm^3	0.04 x 0.04 x 0.04	0.05 x 0.05 x 0.04	0.05 x 0.04 x 0.04	0.05 x 0.05 x 0.05	0.05 x 0.04 x 0.04
2θ range, deg.	2.415-36.273	2.416-36.314	2.389-40.265	2.426-36.252	2.429-36.306
Reflections collected	19667	20122	30408	19360	19418
Data/parameters /restraints	1486/38/1	1491/38/1	1493/38/1	1491/38/1	1489/38/1
R_{int}	0.0294	0.0369	0.0322	0.0348	0.0316
Goodness of fit	1.259	1.206	1.217	1.311	1.229
$R_1(I > 2\sigma(I))$	0.0110	0.0098	0.0095	0.0136	0.0102
wR_2 (all data)	0.0260	0.0221	0.0209	0.0329	0.0242

Chemical formula	$Tm_3Fe_{0.5}SiS_7$	$Tm_3Co_{0.5}SiS_7$	$Tm_3Ni_{0.5}SiS_7$	$Yb_3Fe_{0.5}SiS_7$	$Yb_3Co_{0.5}SiS_7$	$Yb_3Ni_{0.5}SiS_7$
Formula weight	787.30	788.77		800.06	801.09	800.58
Crystal system	Hexagonal					
Space group, Z	*P6₃*	*P6₃*	*P6₃*	*P6₃*	*P6₃*	*P6₃*
a, Å	9.6497(2)	9.6400(3)	9.7107010)	9.5946(2)	9.5543(2)	9.8256(3)
c, Å	5.6801(2)	5.6838(3)	5.65080(10)	5.7211(2)	5.7902(2)	5.6484(2)
V, $Å^3$	458.05(2)	457.43(3)	461.468(13)	456.10(2)	457.74(2)	472.25(3)
ρ_{calcd}, g/cm^3	5.708	5.929	2.815	5.825	5.812	5.633
Radiation (λ, Å)	Mo-Kα (0.710173 Å)					
μ, mm^{-1}	31.210	31.366	214.709	32.924	32.918	32.035
T, K	297.7	299.34	297.67	297.38	298.20	298
Crystal dim., mm^3	0.05 x 0.05 x 0.05	0.05 x 0.05 x 0.05	0.05 x 0.04 x 0.04	0.05 x 0.05 x 0.05	0.04 x 0.04 x 0.04	0.07 x 0.06 x 0.05
2*θ* range, deg.	2.437-36.337	2.440-36.335	2.389-40.265	2.426-36.252	2.462-36.305	2.394-36.313
Reflections collected	21187	19190	30408	19426	19448	20262
Data/parameters/ restraints	1483/38/1	1478/39/1	1493/38/1	1472/39/1	1474/39/1	1518/39/1
R_{int}	0.0456	0.0314	0.0322	0.0385	0.0336	0.0339
Goodness of fit	1.203	1.297	1.217	1.245	1.178	1.189
$R_1(I > 2\sigma(I))$	0.0129	0.0159	0.0095	0.0129	0.0162	0.0149
wR_2 (all data)	0.0275	0.0409	0.0209	0.0292	0.0389	0.0385

Powder X-ray Diffraction (PXRD)

Powder X-ray diffraction (PXRD) data were collected using a powder sample of $RE_3TM_{0.5}SiS_7$ obtained by the solid-state synthesis. These patterns can be seen in figures 3.1-3.17 Data were collected on a Bruker D2 PHASER diffractometer using Cu Kα radiation over a 2θ range 10–65° with a step size of 0.02°.

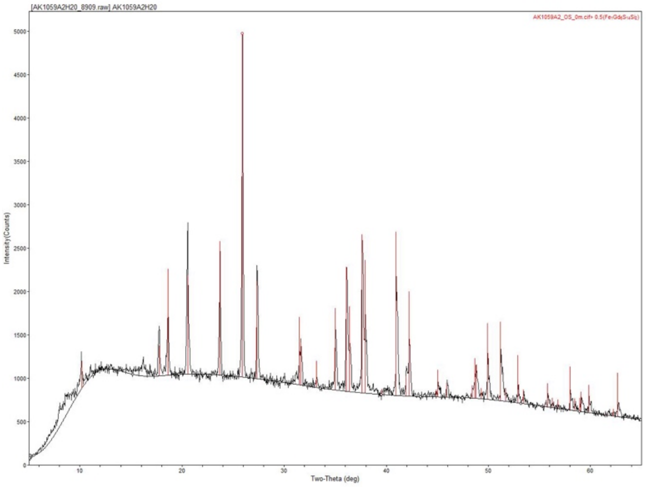

Figure 3.1 Powder X-ray diffraction pattern for $Gd_3Fe_{0.5}SiS_7$ used for SHG measurement. Data are shown in black and peak positions calculated using the single crystal cif file are shown in red.

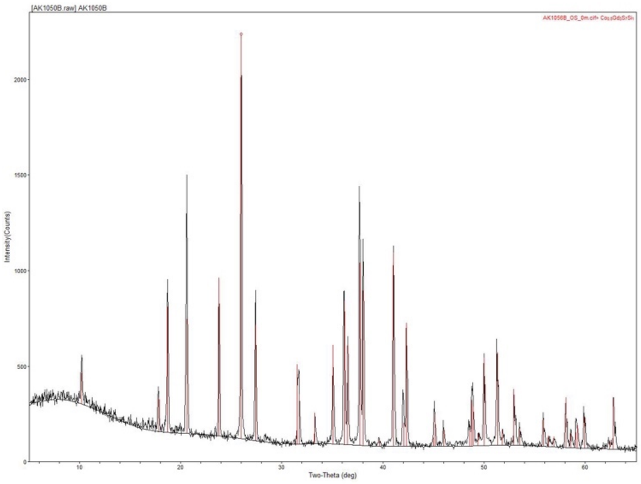

Figure 3.2 Powder X-ray diffraction pattern for $Gd_3Co_{0.5}SiS_7$ used for SHG measurement. Data are shown in black and peak positions calculated using the single crystal cif file are shown in red

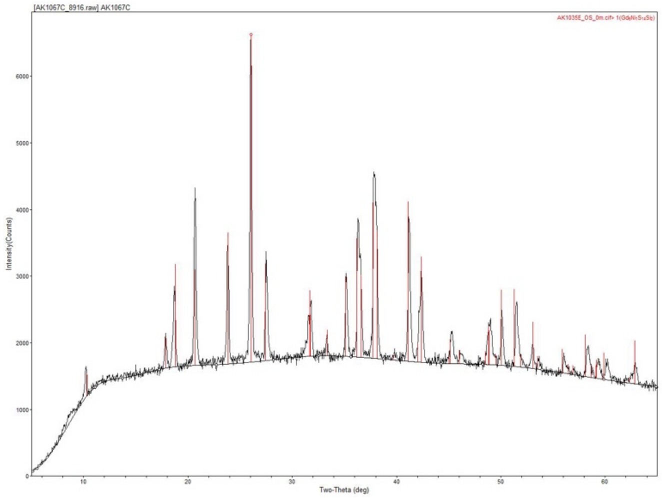

Figure 3.3 Powder X-ray diffraction pattern for $Gd_3Ni_{0.5}SiS_7$ used for SHG measurement. Data are shown in black and peak positions calculated using the single crystal cif file are shown in red.

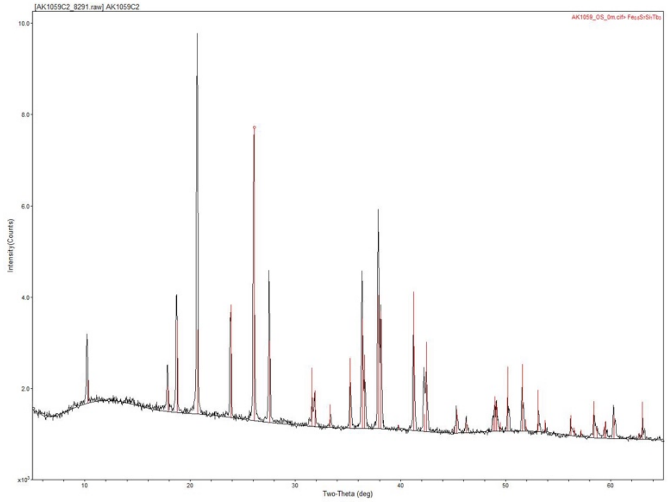

Figure 3.4 Powder X-ray diffraction pattern for $Tb_3Fe_{0.5}SiS_7$ used for SHG measurement. Data are shown in black and peak positions calculated using the single crystal cif file are shown in red.

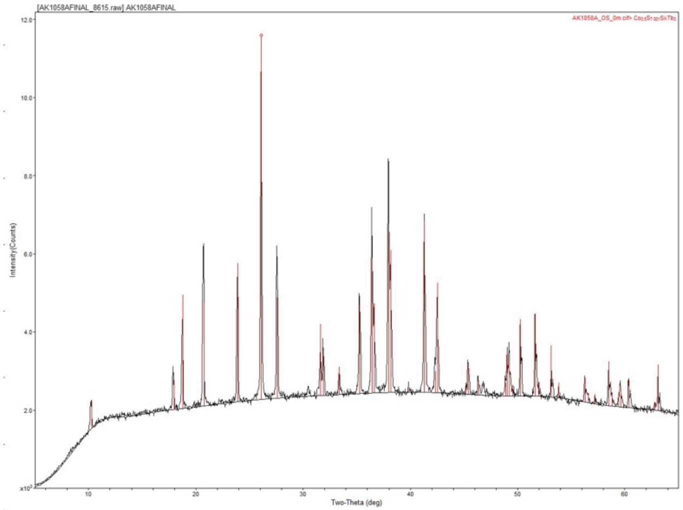

Figure 3.5 Powder X-ray diffraction pattern for $Tb_3Co_{0.5}SiS_7$ used for SHG measurement. Data are shown in black and peak positions calculated using the single crystal cif file are shown in red.

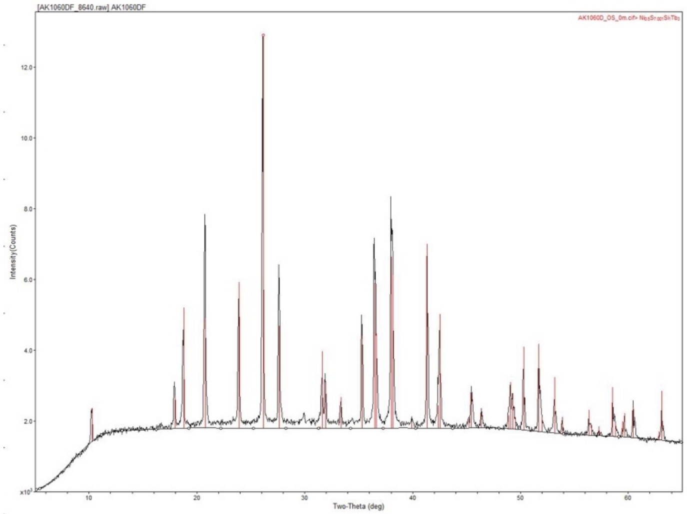

Figure 3.6 Powder X-ray diffraction pattern for $Tb_3Ni_{0.5}SiS_7$ used for SHG measurement. Data are shown in black and peak positions calculated using the single crystal cif file are shown in red.

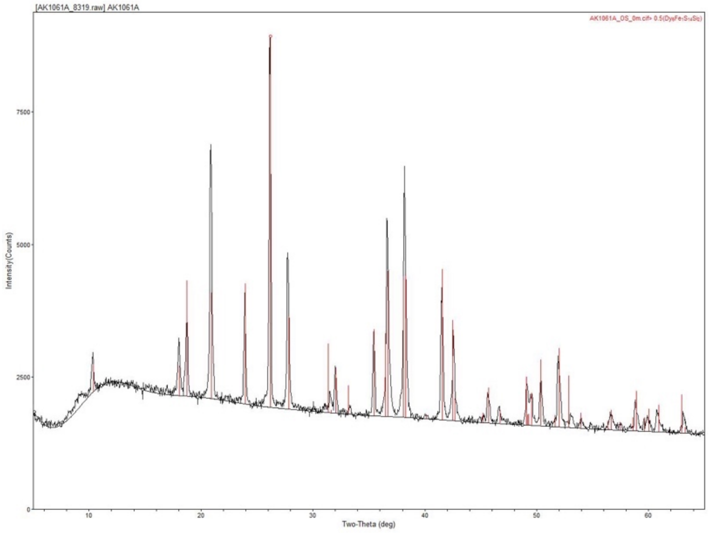

Figure 3.7 Powder X-ray diffraction pattern for $Dy_3Fe_{0.5}SiS_7$ used for SHG measurement. Data are shown in black and peak positions calculated using the single crystal cif file are shown in red

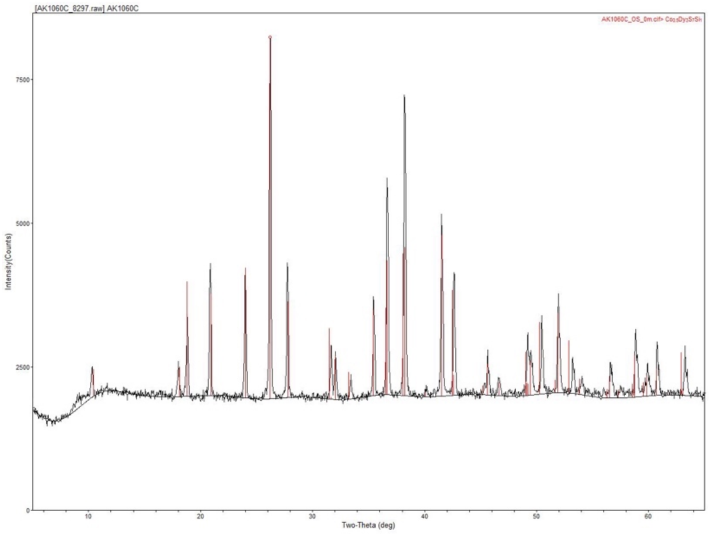

Figure 3.8 Powder X-ray diffraction pattern for $Dy_3Co_{0.5}SiS_7$ used for SHG measurement. Data are shown in black and peak positions calculated using the single crystal cif file are shown in red.

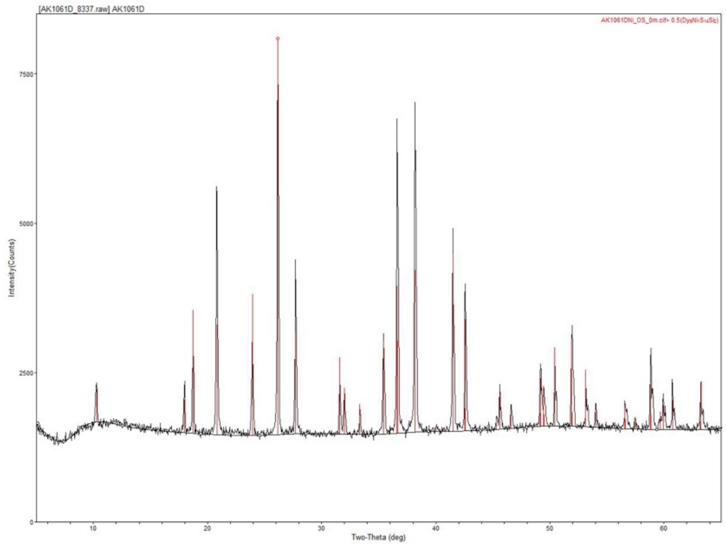

Figure 3.9 Powder X-ray diffraction pattern for $Dy_3Ni_{0.5}SiS_7$ used for SHG measurement. Data are shown in black and peak positions calculated using the single crystal cif file are shown in red.

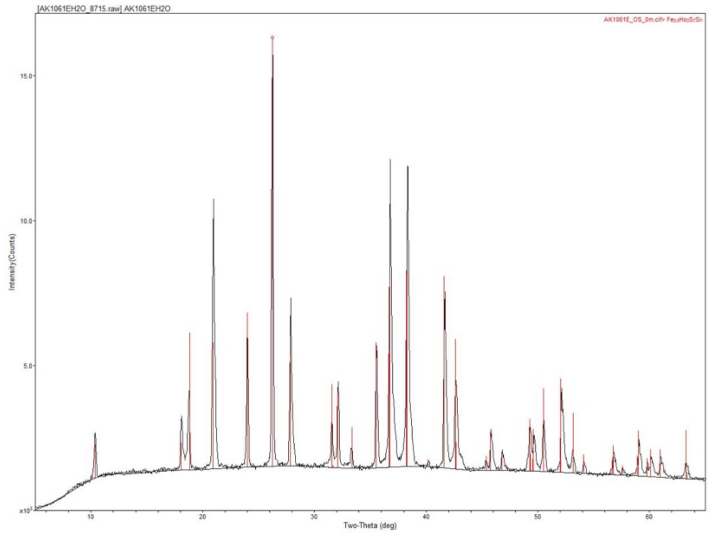

Figure 3.10 Powder X-ray diffraction pattern for $Ho_3Fe_{0.5}SiS_7$ used for SHG measurement. Data are shown in black and peak positions calculated using the single crystal cif file are shown in red.

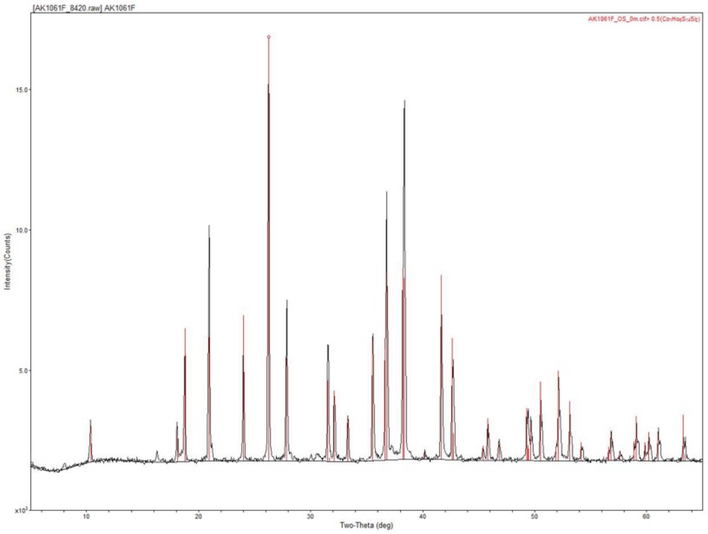

Figure 3.11 Powder X-ray diffraction pattern for $Ho_3Co_{0.5}SiS_7$ used for SHG measurement. Data are shown in black and peak positions calculated using the single crystal cif file are shown in red

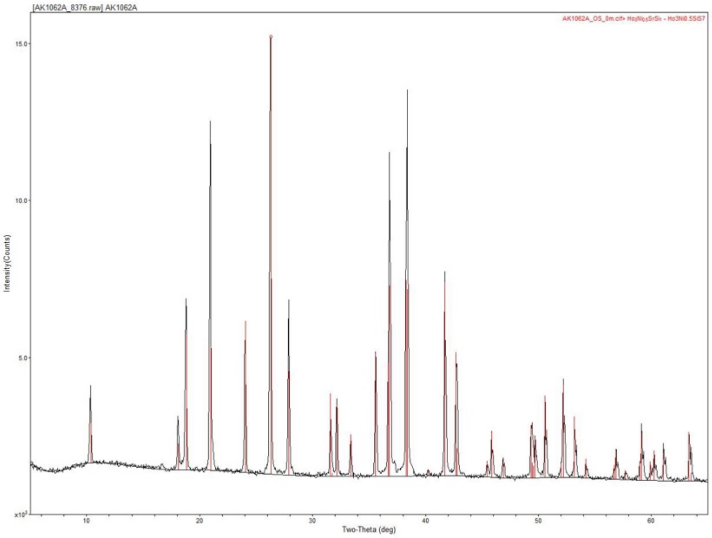

Figure 3.12 Powder X-ray diffraction pattern for $Ho_3Ni_{0.5}SiS_7$ used for SHG measurement. Data are shown in black and peak positions calculated using the single crystal cif file are shown in red.

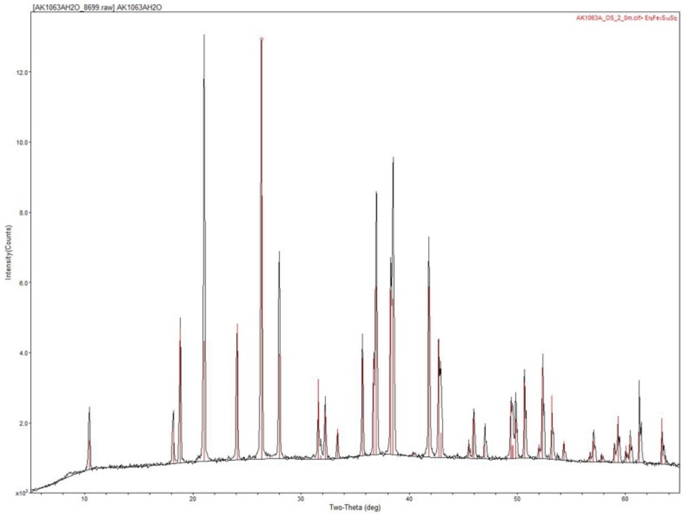

Figure 3.13 Powder X-ray diffraction pattern for $Er_3Fe_{0.5}SiS_7$ used for SHG measurement. Data are shown in black and peak positions calculated using the single crystal cif file are shown in red.

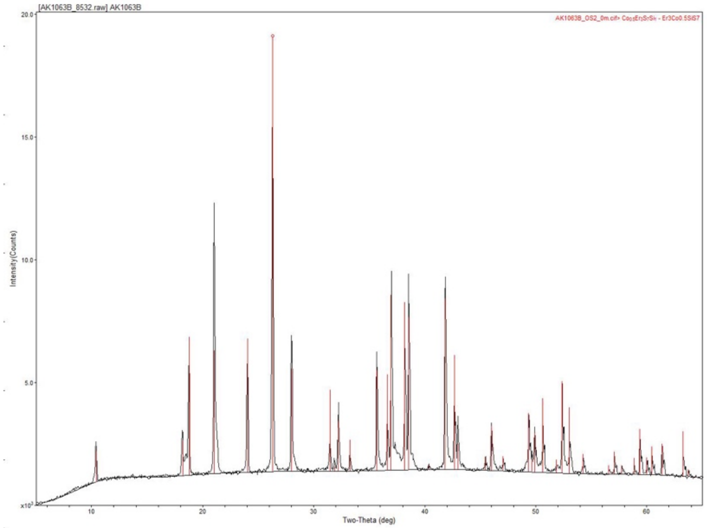

Figure 3.14 Powder X-ray diffraction pattern for $Er_3Co_{0.5}SiS_7$ used for SHG measurement. Data are shown in black and peak positions calculated using the single crystal cif file are shown in red.

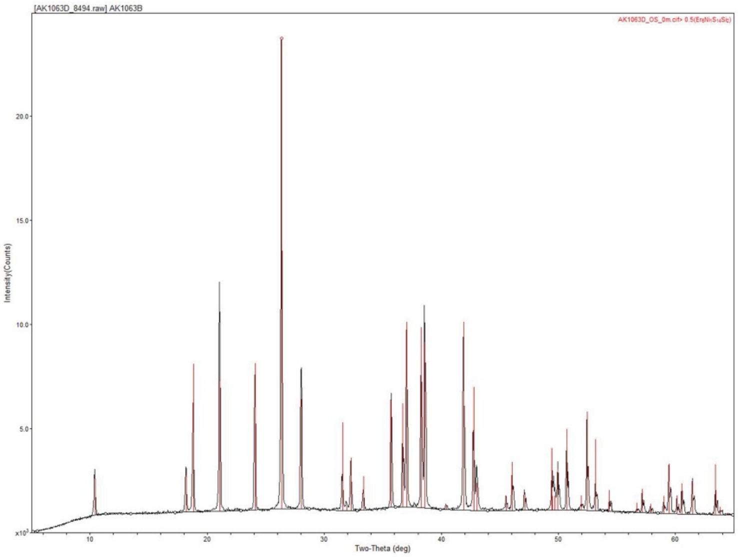

Figure 3.15 Powder X-ray diffraction pattern for $Er_3Ni_{0.5}SiS_7$ used for SHG measurement. Data are shown in black and peak positions calculated using the single crystal cif file are shown in red.

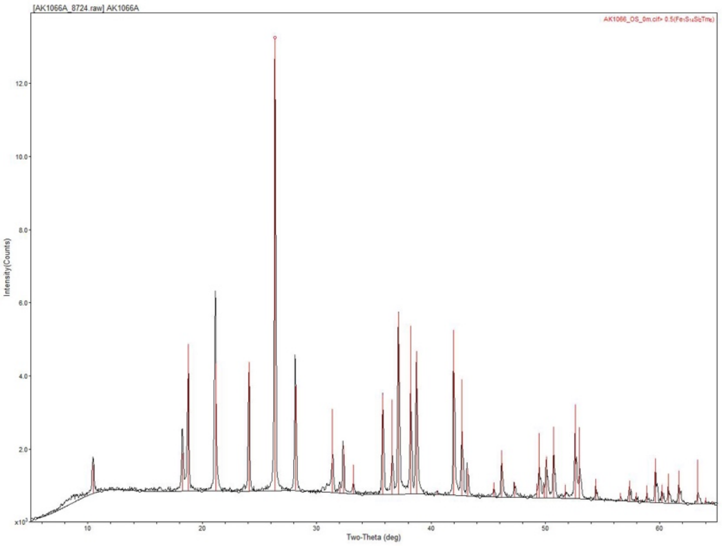

Figure 3.16 Powder X-ray diffraction pattern for $Tm_3Fe_{0.5}SiS_7$ used for SHG measurement. Data are shown in black and peak positions calculated using the single crystal cif file are shown in red.

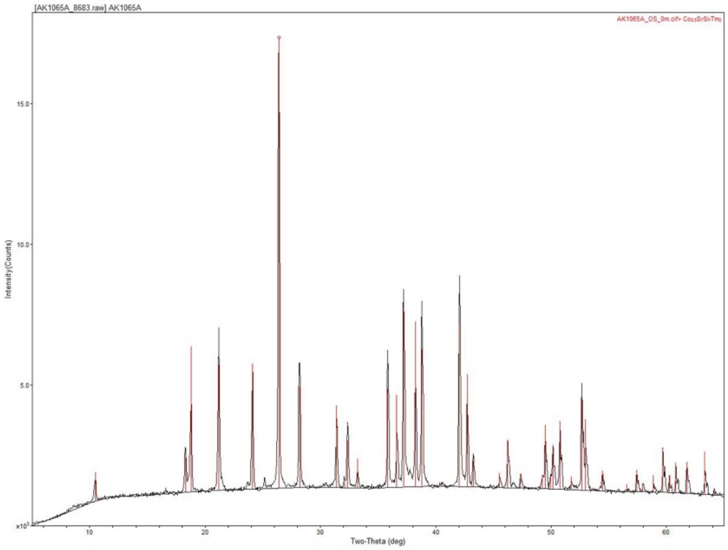

Figure 3.17 Powder X-ray diffraction pattern for $Tm_3Co_{0.5}SiS_7$ used for SHG measurement. Data are shown in black and peak positions calculated using the single crystal cif file are shown in red.

Magnetic Susceptibility

Magnetic property measurements for $RE_3TM_{0.5}SiS_7$ (RE= Gd-Tm, T= Fe, Co, Ni) were performed using a Quantum Design magnetic property measurement system (QD MPMS 3 SQUID Magnetometer). The magnetic susceptibility was measured under zero-field-cooled (zfc) and field-cooled (fc) conditions from 2 to 300 K in an applied magnetic field of 0.1 T. Magnetization as a function of applied field was measured from −5 to 5 T at 2 K. Data were corrected for the sample shape and radial offset effects as described previously.[29]

Synthesis

Much interest has been shown in the $RE_3M_{0.5}MQ_7$ phase due to its structural and compositional diversity. First discovered by Michelet and Flahaut in 1969 and expanded on by Collin and Laruelle in the early 1970s.[30-32] This phase has seen a dramatic increase in research and development since the beginning of the 21st century. This includes our previous contribution of the $RE_3Mg_{0.5}SiS_7$ analogs. Throughout our synthesis of these structures, we noticed the ease at which this structure forms and its resiliency to form with very little impurity phases due to the use of the BCM method. We decided to attempt to expand this research to a greater degree, with the inclusion of transition metals for an interest in their magnetic properties. As well as expand the phase space of these compositions by showing Ytterbium could be added to the series. The synthesis of the $RE_3TM_{0.5}SiS_7$ (RE= Gd-Yb; TM=Fe, Co, Ni) series was performed using NaI as a flux and using boron powder to remove the oxygen from our RE_2O_3 reagents, we successfully obtained high quality single crystals for all the target compositions.

Minor impurities that could not be indexed were found in the samples after workup with methanol. Samples were then quickly washed with water, removing the impurities, resulting in phase pure samples.

Crystal Structure

The crystal structure of the $RE_3TM_{0.5}SiS_7$ (RE= Gd-Yb; TM= Fe, Co, Ni) are all isostructural with our previously reported $RE_3Mg_{0.5}SiS_7$ compounds. These compounds crystallize in the hexagonal crystal system taking on the space group $P6_3$. In this structure the rare earth coordination environment consists of RES_8 bi-capped trigonal prisms that edge and corner share to create a ring-like assembly. These columns form a ring like structure, spiraling around the TMS_6 face-sharing octahedra. Six isolated SiS_4 tetrahedra sit around the ring like structures of RES_8 bi-capped trigonal prisms. These isolated SiS_4 tetrahedra another ring around the RES_8 bi-capped trigonal prism. Figure 3.18 shows the 3D framework structure of the reported compounds.

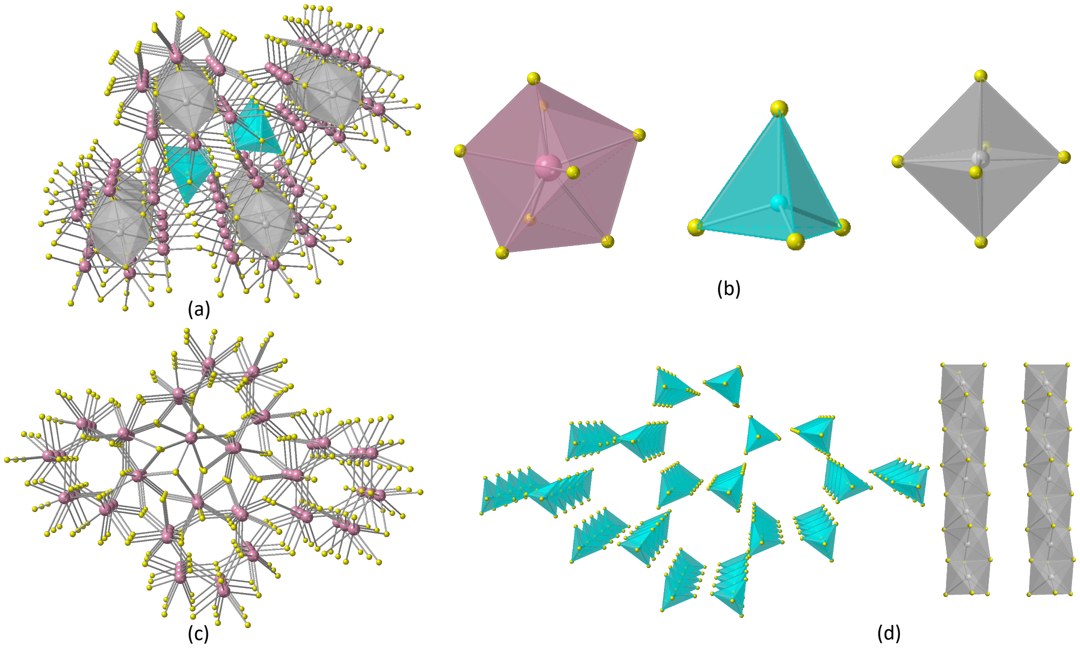

Figure 3.18 (a) 3D framework structure of $Dy_3Ni_{0.5}SiS_7$ viewed down the c-direction (b) Dy, Si, and Ni coordination environments (c) DyS_8 chains developing the framework (d) isolated SiS_4 tetrahedra in ring like formation and face-sharing MgS_6 octahedra.

Magnetic Properties

The results from the magnetic property measurements for all title compounds are shown in figures 3.19-3.21. Using the high temperature region of the inverse susceptibility vs temperature plot the data were fit to the Curie Weiss (CW) Law to obtain the molar magnetic susceptibility and the Weiss constant, the results are summarized in table 3.2. Good agreement was found between the calculated and measured magnetic moments for all the compounds. All the Weiss constants are slightly negative, indicating the presence of weak antiferromagnetic (AF) interactions, consistent with the low AF transition temperatures. 10 of the new compositions display a clear antiferromagnetic transition in the temperature range of 2-14 K in the molar magnetic susceptibility vs. temperature plots, while for 7 compositions no AF transitions are evident in the susceptibility plot. Several compositions exhibit an upturn in the susceptibility plot below the AF transition. This could be due to a curie tail or possibly a 2nd magnetic transition. In table 3.2, the larger number refers to the AF transition while the smaller number (if present) refers to the temperature at which the susceptibility increases again.

There is no clear trend as to which compositions exhibit an AF transition in the susceptibility data and which do not. In all cases both the rare earth cation and the transition metal cation have unpaired electrons that could, in principle, result in an AF transition. It is, however, most likely that the compositions that do not exhibit an obvious AF transition down to 2 K simple undergo an AF transition at temperatures that fall below the lowest temperature measured.

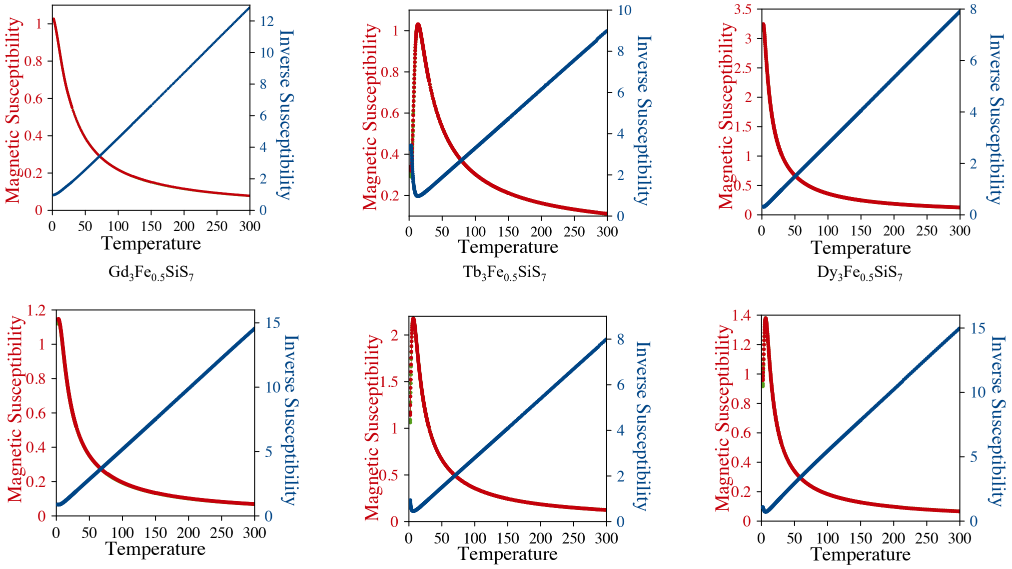

$Gd_3Fe_{0.5}SiS_7$ $Tb_3Fe_{0.5}SiS_7$ $Dy_3Fe_{0.5}SiS_7$

$Ho_3Fe_{0.5}SiS_7$ $Er_3Fe_{0.5}SiS_7$ $Tm_3Fe_{0.5}SiS_7$

Figure 3.19 Magnetic and Inverse Susceptibility vs Temperature Plots for $RE_3Fe_{0.5}SiS_7$ (RE=Gd-Tm)

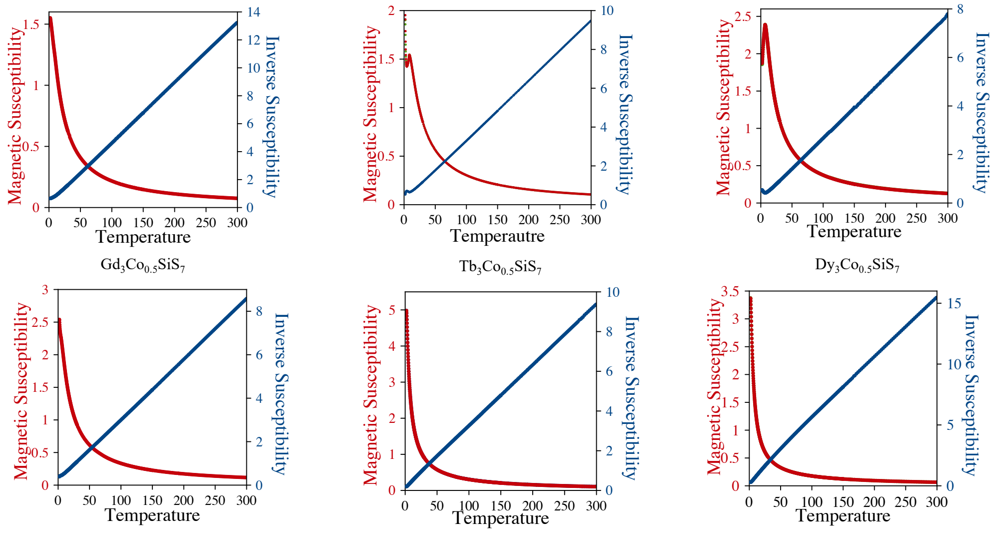

$Gd_3Co_{0.5}SiS_7$ $Tb_3Co_{0.5}SiS_7$ $Dy_3Co_{0.5}SiS_7$

$Ho_3Co_{0.5}SiS_7$ $Er_3Co_{0.5}SiS_7$ $Tm_3Co_{0.5}SiS_7$

Figure 3.20 Magnetic and Inverse Susceptibility vs Temperature Plots for $RE_3Co_{0.5}SiS_7$ (RE=Gd-Tm)

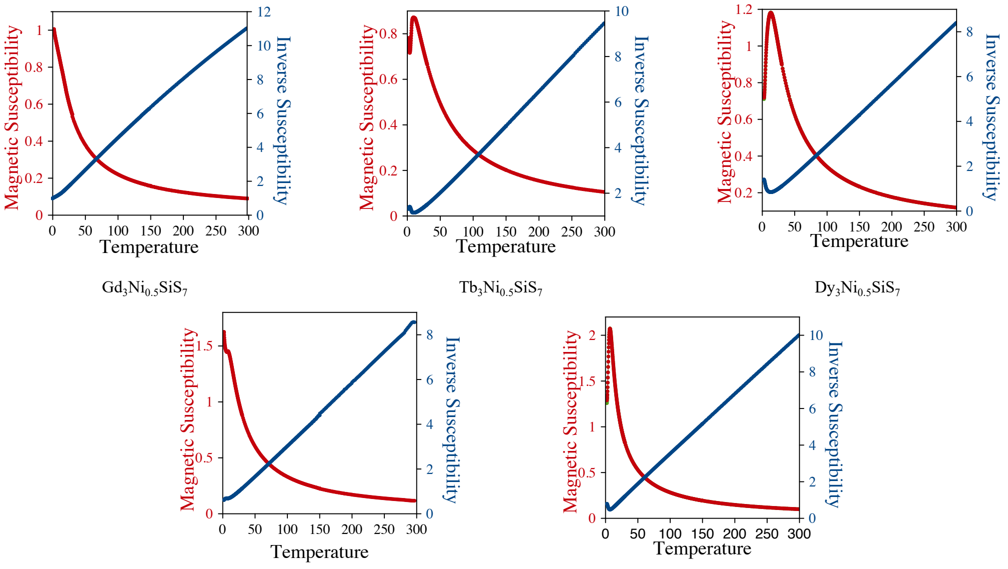

$Gd_3Ni_{0.5}SiS_7$ $Tb_3Ni_{0.5}SiS_7$ $Dy_3Ni_{0.5}SiS_7$

$Ho_3Ni_{0.5}SiS_7$ $Er_3Ni_{0.5}SiS_7$

Figure 3.21 Magnetic and Inverse Susceptibility vs Temperature Plots for $RE_3Ni_{0.5}SiS_7$ (RE=Gd-Er)

Table 3.2 Magnetic data for all target compounds

Compound	Observed μ_{eff} (μ_B/Ln^{3+}) from Curie–Weiss fit (200–300 K)	calculated μ_{eff} (μ_B/Ln^{3+})	Θ_W (K)	T_n (K)
$Gd_3Fe_{0.5}SiS_7$	14.18	13.80	-9	N/A
$Gd_3Co_{0.5}SiS_7$	13.60	13.78	-7	N/A
$Gd_3Ni_{0.5}SiS_7$	13.45	13.76	-14	N/A
$Tb_3Fe_{0.5}SiS_7$	16.75	16.83	-15	2.7; 13.5
$Tb_3Co_{0.5}SiS_7$	16.03	16.82	-6	4.5; 8.5
$Tb_3Ni_{0.5}SiS_7$	16.24	16.81	-13	3.5; 8.3
$Dy_3Fe_{0.5}SiS_7$	17.61	18.48	-7	2.9
$Dy_3Co_{0.5}SiS_7$	17.64	18.42	-4	6.9
$Dy_3Ni_{0.5}SiS_7$	17.05	18.41	-6	2.5; 13.3
$Ho_3Fe_{0.5}SiS_7$	17.21	18.41	-7	N/A
$Ho_3Co_{0.5}SiS_7$	16.90	18.39	-6	N/A
$Ho_3Ni_{0.5}SiS_7$	17.00	18.38	-8	6.7; 8.1
$Er_3Fe_{0.5}SiS_7$	17.54	16.50	-7	6.7
$Er_3Co_{0.5}SiS_7$	16.14	16.48	-6	N/A
$Er_3Ni_{0.5}SiS_7$	15.71	16.47	-9	6.9
$Tm_3Fe_{0.5}SiS_7$	12.94	13.23	-14	6.5
$Tm_3Co_{0.5}SiS_7$	12.75	13.21	-16	N/A

It is of interest to compare the magnetic behavior of the $RE_3TM_{0.5}SiS_7$ phases with their $RE_3TM_{0.5}SiS_7$ analogs that have been reported. However, in the latter cases, magnetic properties were reported for only a few compositions, specifically, $RE_3TM_{0.5}SiS_7$ (RE = Gd, Dy, Er, Tm), $RE_3TM_{0.5}SiS_7$ (RE = Gd, Tb, Dy, Er, Tm) and $Gd_3Co_{0.5}SiS_7$, all published by Daszkiewicz et al.[17, 18] For these germanate analogs, also, the AF transition temperatures are very low and generally in line with those observed for the silicates. No magnetic structures were reported for the germanates, and hence, it would be of interest to determine the magnetic structures of both silicates and germanates using neutron diffraction to compare their magnetic structures. This is planned for the future. The versatility of this extended family of chalcometallates is due to the ease with which a wide range of transition and rare earth metal cations can be incorporated, coupled with the ability to change from thiosilicates to thiogermanates, which impacts the lattice parameters of the structure. This enables the modification of their physical properties, both magnetic and optical, by the judicious choice of elemental constituents. It is expected that further compositions can be prepared by expanding this series to VS4, PS4, and SnS4 compositions in the future.

Conclusion

Through the combination of the BCM method and molten flux crystal growth, high quality single crystals of $RE_3TM_{0.5}SiS_7$ (RE= Gd-Yb, TM= Fe, Co, Ni) were prepared for single crystal X-ray analysis. Phase pure products of the target phases were obtained by washing samples in water to dissolve impurities. This allowed for magnetic property measurements of the target phases. As we have two magnetic elements in the crystal lattice, unique magnetism is reported on stemming from the rare earths and transition metals magnetic sublattices. Magnetic susceptibility measurements showed the target compounds exhibit antiferromagnetic behavior down to 2 K.

The continued synthesis of novel of chalcogenide compounds is of upmost importance as they continue to show potentials in all aspects of desired physical properties. Novel synthetic methods to reach these compounds must be utilized and improved upon. Overall, we have again demonstrated the effectiveness and tested the limitations of the novel BCM method for the synthesis of the $RE_xM_xMS_7$ family.

ACKNOWLEDGMENTS

Research supported by the US Department of Energy, Office of Basic Energy Sciences, Division of Materials Sciences and Engineering under award DE-SC0018739. Synthesis, structural characterization, and magnetic studies performed at UofSC.

References

1. Priyadarshini, P.; Sahoo, D.; Naik, R. A review on the optical properties of some germanium based chalcogenide thin films and their applications. *Opt. Quantum Electron.* ***2022,*** *54,*
2. Sahoo, D.; Naik, R. A review on the linear/nonlinear optical properties of Se doped chalcogenide thin films as potential optoelectronic applications. *J. Non-Cryst. Solids.* ***2022,*** *597, 121934.*
3. Kanatzidis, M. G. Discovery-Synthesis, Design, and Prediction of Chalcogenide Phases. *Inorg. Chem.* ***2017,*** *56, 3158-3173.*
4. Zhen, N.; Nian, L.; Li, G.; Wu, K.; Pan, S. A High Laser Damage Threshold and a Good Second-Harmonic Generation Response in a New Infrared NLO Material: $LiSm_3SiS_7$. *Crystals.* ***2016,*** *6, 121.*
5. Kamaya, N.; Homma, K.; Yamakawa, Y.; Hirayama, M.; Kanno, R.; Yonemura, M.; Kamiyama, T.; Kato, Y.; Hama, S.; Kawamoto, K.; Mitsui, A. A lithium superionic conductor. *Nat. Mater.* ***2001,*** *158, 682-686.*
6. Kanno, R.; Murayama, M. Lithium Ionic Conductor Thio-LISICON: The Li_2S-GeS_2-P_2S_5 System. *Nat. Mater.* ***2011,*** *148, A742.*
7. Iwanczyk, J. S.; Nygård, E.; Meirav, O.; Arenson, J.; Barber, W. C.; Hartsough, N. E.; Malakhov, N.; Wessel, J. C. Photon Counting Energy Dispersive Detector Arrays for X-ray Imaging. *IEEE Trans. Nucl. Sci.* ***2009,*** *56, 535-542.*
8. Rogalski, A. HgCdTe infrared detectro material: history, status and outlook. *Rep. Prog. Phys.* ***2005,*** *68, 2267-2336.*
9. Watanabe, S.; Ishikawa, S.-n.; Aono, H.; Takeda, S.; Odaka, H.; Kokubun, M.; Takahashi, T.; Nakazawa, K.; Tajima, H.; Onishi, M.; Kuroda, Y. High Energy Resolution Hard X-Ray and Gamma-Ray Imagers Using CdTe Diode Devices. *IEEE Trans. Nuc. Sci.* ***2009,*** *56, 777-782.*
10. Bera, T. K.; Jang, J. I.; Ketterson, J. B.; Kanatzidis, M. G. Strong second harmonic generation from the tantalum thioarsenates $A_3Ta_2AsS_{11}$ (A = K and Rb). *J. Am. Chem. Soc.* ***2009,*** *131, 75-77.*
11. Bera, T. K.; Jang, J. I.; Song, J. H.; Malliakas, C. D.; Freeman, A. J.; Ketterson, J. B.; Kanatzidis, M. G. Soluble semiconductors $AAsSe_2$ (A = Li, Na) with a direct-band-gap and strong second harmonic generation: a combined experimental and theoretical study. *J. Am. Chem. Soc.* ***2010,*** *132, 3484-3495.*
12. Lekse, J. W.; Moreau, M. A.; McNerny, K. L.; Yeon, J.; Halasyamani, P. S.; Aitken, J. A. Second-harmonic generation and crystal structure of the diamond-like semiconductors Li_2CdGeS_4 and Li_2CdSnS_4. *Inorg. Chem.* ***2009,*** *48, 7516-7518.*
13. Babo, J. M.; Choi, E. S.; Albrecht-Schmitt, T. E. Synthesis, structure, magnetism, and optical properties of $Cs_2Cu_3DyTe_4$. *Inorg. Chem.* ***2012,*** *51, 11730-11735.*
14. Caron, J. M.; Neilson, J. R.; Miller, D. C.; Llobet, A.; McQueen, T. M. Iron displacements and magnetoelastic coupling in the antiferromagnetic spin-ladder compound $BaFe_2Se_3$. *Phys. Rev. B.* ***2011,*** *84,*
15. King, A. A.; Breton, L. S.; Morrison, G.; Smith, M. D.; Liang, M.; Halasyamani, P. S.; Zur Loye, H.-C. Crystal Structures and Property Measurements of Rare Earth Magnesium Thiosilicates Synthesized via Flux Crystal Growth Utilizing the Boron Chalcogen Mixture (BCM) Method. *Inorg. Chem.* ***2023,*** *62, 7446-7452.*

16. Zhou, Y.; Iyer, A. K.; Oliynyk, A. O.; Heyberger, M.; Lin, Y.; Qiu, Y.; Mar, A. Quaternary rare-earth sulfides $RE_3M_{0.5}M'S_7$ (M = Zn, Cd; M′ = Si, Ge). *J. Solid State Chem.* ***2019,*** *278, 120914.*
17. Daszkiewicz, M.; Pashynska, Y. O.; Marchuk, O. V.; Gulay, L. D.; Kaczorowski, D. Crystal structure and magnetic properties of $R_3Fe_{0.5}GeS_7$ (R = Y, La, Ce, Pr, Sm, Gd, Tb, Dy, Ho, Er and Tm). *J. Alloys Compd.* ***2014,*** *616, 243-249.*
18. Daszkiewicz, M.; Pashynska, Y. O.; Marchuk, O. V.; Gulay, L. D.; Kaczorowski, D. Crystal structure and magnetic properties of $R_3Co_{0.5}GeS_7$ (R = Y, La, Ce, Pr, Nd, Sm, Gd, Tb, Dy, Ho, Er and Tm) and $R_3Ni_{0.5}GeS_7$ (R = Y, Ce, Sm, Gd, Tb, Dy, Ho, Er and Tm). *J. Alloys Compd.* ***2015,*** *647, 445-455.*
19. Gulay, L. D.; Olekseyuk, I. D.; Wołcyrz, M.; Stępień-Damm, J. The Crystal Structures of R_3CuSnS_7 (R = La-Nd, Sm, Gd-Ho). *Z. anorg. allg. Chem.* ***2005,*** *631, 1919-1923.*
20. Gulay, L. D.; Kaczorowski, D.; Pietraszko, A. Crystal structure and magnetic properties of $Ce_3CuSnSe_7$. *J. Alloys Compd.* ***2005,*** *403, 49-52.*
21. Guo, S. P.; Guo, G. C.; Wang, M. S.; Zou, J. P.; Xu, G.; Wang, G. J.; Long, X. F.; Huang, J. S. A series of new infrared NLO semiconductors, $ZnY_6Si_2S_{14}$, $Al_xDy_3(Si_{y)}Al_{1-y})S_7$, and $Al_{0.33}Sm_3SiS_7$. *Inorg. Chem.* ***2009,*** *48, 7059-7065.*
22. He, J.; Wang, Z.; Zhang, X.; Cheng, Y.; Gong, Y.; Lai, X.; Zheng, C.; Lin, J.; Huang, F. Synthesis, structure, magnetic and photoelectric properties of $Ln_3M_{0.5}M'Se_7$ (Ln = La, Ce, Sm; M = Fe, Mn; M′ = Si, Ge) and $La_3MnGaSe_7$. *RSC Advances.* ***2015,*** *5, 52629-52635.*
23. Iyer, A. K.; Yin, W.; Lee, E. J.; Lin, X.; Mar, A. Quaternary rare-earth sulfides $RE_3M_{0.5}GeS_7$ (RE=La–Nd, Sm; M=Co, Ni) and $Y_3Pd_{0.5}SiS_7$. *J. Solid State Chem.* ***2017,*** *250, 14-23.*
24. Melnychuk, K.; Marchuk, O.; Daszkiewicz, M.; Gulay, L. Crystal structure of novel $R_3Fe(Co, Ni)_{0.5}SnS_7$ (R = Y, La, Ce, Pr, Nd, Sm, Gd, Tb, Dy and Ho) compounds. *Struct. Chem.* ***2020,*** *31, 1945-1957.*
25. Akopov, G.; Hewage, N. W.; Yox, P.; Viswanathan, G.; Lee, S. J.; Hulsebosch, L. P.; Cady, S. D.; Paterson, A. L.; Perras, F. A.; Xu, W.; Wu, K.; Mudryk, Y.; Kovnir, K. Synthesis-enabled exploration of chiral and polar multivalent quaternary sulfides. *Chem. Sci.* ***2021,*** *12, 14718-14730.*
26. Krause, L.; Herbst-Irmer, R.; Sheldrick, G. M.; Stalke, D. Comparison of silver and molybdenum microfocus X-ray sources for single-crystal structure determination. *J Appl. Crystallogr.* ***2015,*** *48, 3-10.*
27. Sheldrick, G. M. *Shelxt*– Integrated Space-Group and Crystal-Structure Determination. *Acta Crystallogr. A.* ***2015,*** *71, 3-8.*
28. Hübschle, C. B.; Sheldrick, G. M.; Dittrich, B. ShelXle: a Qt graphical user interface for SHELXL. *J Appl. Crystallog.* ***2011,*** *44, 1281-1284.*
29. Morrison, G.; zur Loye, H.-C. Simple Correction for the Sample Shape and Radial Offset Effects on SQUID Magnetometers: Magnetic Measurements on Ln_2O_3(Ln=Gd, Dy, Er) Standards. *J. Solid State Chem.* ***2015,*** *221, 334-337.*
30. Collin G.; Laurelle, P. Structure cristalline de $La_6MnSi_2S_{14}$. *C. R. Acad. Sci. Ser. C.* ***1970,*** *270, 410-412.*
31. Collin G.; Laurelle, P. Structure de $La_6Cu_2Si_2S_{14}$. *Bull. Soc. Fr. Mineral. Cristallogr.* ***1971,*** *94, 175-176.*

32. Michelet, A.; Flahaut, J. Sur les composés du type $La_6MnSi_2S_{14}$. *C. R. Acad. Sci. Ser. C.* ***1969,*** *269 , 1203-1205.*

References

Chapter 1

1. Kanatzidis, M. G. Discovery-Synthesis, Design, and Prediction of Chalcogenide Phases. *Inorg. Chem.* ***2017,*** *56, 3158-3173.*
2. Krebs, B. Thio- and Seleno-Compounds of Main Group Elements?Novel Inorganic Oligomers and Polymers. *Angew. Chem. Int. Ed. Engl.* ***1983,*** *22, 113-134.*
3. Dziaugys, A.; Banys, J.; Macutkevic, J.; Sobiestianskas, R.; Vysochanskii, Y. Dipolar glass phase in ferrielectrics: $CuInP_2S_6$and $Ag_{0.1}Cu_{0.9}InP_2$ S_6crystal. *Physica. status. solidi (a).* ***2010,*** *207, 1960-1967.*
4. Lacroix, P. G.; Clément, R.; Nakatani, K.; Zyss, J.; Ledoux, I. Stilbazolium-MPS_3 Nanocomposites with Large Second-Order Optical Nonlinearity and Permanent Magnetization. *Science.* ***1994,*** *263, 658-660.*
5. Gauthier, G.; Jobic, S.; Evain, M.; Koo, H.-J.; Whangbo, M.-H.; Fouassier, C.; Brec, R. Syntheses, Structures, and Optical Properties of Yellow Ce_2SiS_5, $Ce_6Si_4S_{17}$, and $Ce_4Si_3S_{12}$ Materials. *Chem. Mater.* ***2003,*** *15, 828-837.*
6. Huang, W.; Matsui, N.; Hori, S.; Suzuki, K.; Hirayama, M.; Yonemura, M.; Saito, T.; Kamiyama, T.; Sasaki, Y.; Yoon, Y.; Kim, S.; Kanno, R. Anomalously High Ionic Conductivity of Li_2SiS_3-Type Conductors. *J. Am. Chem. Soc.* ***2022,*** *144, 4989-4994.*
7. Riccardi, R.; Gout, D.; Gauthier, G.; Guillen, F.; Jobic, S; Garcia, A.; Huguenin, D.; Macaudière, P.; Fouassier, C.; Brec, R. Structural Investigation and Luminescence Properties of the $Ce_3(SiS_4)_2X$ (X=Cl, Br, I) Family and the $La_{3-x}Ce_x(SiS_4)_2I$ ($0 \leq x \leq 1$) Solid Solution. *J. Solid State Chem.* ***1999,*** *147, 259-268.*
8. Li, G. M.; Chu, Y.; Li, J.; Zhou, Z. X. Li_2CdSiS_4, a promising IR NLO material with a balanced E_g and SHG response originating from the effect of Cd with d^{10} configuration. *Dalton Trans.* ***2020,*** *49, 1975-1980.*
9. Lee, S. P.; Chan, T. S.; Chen, T. M. Novel reddish-orange-emitting $BaLa_2Si_2S_8:Eu^{2+}$ thiosilicate phosphor for LED lighting. *ACS Appl Mater Interfaces.* ***2015,*** *7, 40-44.*
10. Wu, L. M.; Seo, D. K. New solid-gas metathetical synthesis of binary metal polysulfides and sulfides at intermediate temperatures: utilization of boron sulfides. *J. Am. Chem. Soc.* ***2004,*** *126, 4676-4681.*
11. Huang, Y.-Z.; Chen, L.; Wu, L.-M. Crystalline Nanowires of $Ln_{2<}O_2S$, $Ln_2O_2S_2$, LnS_2 (Ln = La, Nd), and $La_2O_2S:Eu^{3+}$. Conversions via the Boron-Sulfur Method That Preserve Shape. *Crystal. Growth Des.* ***2008,*** *8, 739-743.*
12. Breton, L. S.; Klepov, V. V.; zur Loye, H.-C. Facile Oxide to Chalcogenide Conversion for Actinides Using the Boron-Chalcogen Mixture Method. *J. Am. Chem. Soc.* ***2020,*** *142, 14365-14*

13. Breton, L. S.; Morrison, G.; Lacroix, M. R.; Halasyamani, P. S.; zur Loye, H.-C. Lanthanide thioborates, an emerging class of nonlinear optical materials, efficiently synthesized using the boron-chalcogen mixture method. *Chem. Commun. (Camb).* ***2022,*** *58, 7992-7995*
14. Breton, L. S.; Smith, M. D.; zur Loye, H.-C. Trends in Rare Earth Thiophosphate Syntheses: $Rb_3Ln(PS_4)_2$ (Ln = La, Ce, Pr), $Rb_{3-x}Na_xLn(PS_4)_2$ (Ln = Ce, Pr; $x = 0.50$, 0.55), and $RbEuPS_4$Obtained by Molten Flux Crystal Growth. *CrystEngComm.* ***2021,*** *23, 5241-5248.*
15. Usman, M.; Smith, M. D.; Morrison, G.; Klepov, V. V.; Zhang, W.; Halasyamani, P. S.; zur Loye, H.-C. Molten Alkali Halide Flux Growth of an Extensive Family of Noncentrosymmetric Rare Earth Sulfides: Structure and Magnetic and Optical (SHG) Properties. *Inorg. Chem.* ***2019,*** *58, 8541-8550.*

Chapter 2

1. Kanatzidis, M. G. Discovery-Synthesis, Design, and Prediction of Chalcogenide Phases. *Inorg. Chem.* ***2017,*** *56, 3158-3173.*
2. Breton, L. S.; Smith, M. D.; zur Loye, H.-C. Trends in Rare Earth Thiophosphate Syntheses: $Rb_3Ln(PS_4)_2$ (Ln = La, Ce, Pr), $Rb_{3-x}Na_xLn(PS_4)_2$ (Ln = Ce, Pr; $x = 0.50$, 0.55), and $RbEuPS_4$Obtained by Molten Flux Crystal Growth. *CrystEngComm.* ***2021,*** *23, 5241-5248.*
3. Usman, M.; Smith, M. D.; Morrison, G.; Klepov, V. V.; Zhang, W.; Halasyamani, P. S.; zur Loye, H.-C. Molten Alkali Halide Flux Growth of an Extensive Family of Noncentrosymmetric Rare Earth Sulfides: Structure and Magnetic and Optical (SHG) Properties. *Inorg. Chem.* ***2019,*** *58, 8541-8550.*
4. Breton, L. S.; Morrison, G.; Lacroix, M. R.; Halasyamani, P. S.; zur Loye, H.-C. Lanthanide thioborates, an emerging class of nonlinear optical materials, efficiently synthesized using the boron-chalcogen mixture method. *Chem. Commun.(Camb).* ***2022,*** *58, 7992-7995.*
5. Breton, L. S.; Klepov, V. V.; zur Loye, H.-C. Facile Oxide to Chalcogenide Conversion for Actinides Using the Boron-Chalcogen Mixture Method. *J Am. Chem. Soc.* ***2020,*** *142, 14365-14373.*
6. Wu, L.-M.; Seo, D. K. New solid-gas metathetical synthesis of binary metal polysulfides and sulfides at intermediate temperatures: utilization of boron sulfides. *J. Am. Chem. Soc.* ***2004,*** *126, 4676-4681.*
7. Huang, Y.-Z.; Chen, L.; Wu, L.-M. Crystalline Nanowires of Ln_2O_2S, $Ln_2O_2S_2$, LnS_2 (Ln = La, Nd), and $La_2O_2S:Eu^{3+}$. Conversions via the Boron-Sulfur Method That Preserve Shape. *Cryst. Growth Des.* ***2008,*** *8, 739-743.*
8. Huang, Y.-Z.; Chen, L.; Wu, L.-M. Submicrosized rods, cables, and tubes of ZnE (E = S, Se, Te): exterior-interior boron-chalcogen conversions and optical properties. *Inorg. Chem.* ***2008,*** *47, 10723-10728.*
9. Collin G.; Laurelle, P. Structure de $La_6Cu_2Si_2S_{14}$. *Bull. Soc. Fr. Mineral. Cristallogr.* ***1971,*** *94, 175-176.*

10. Daszkiewicz, M.; Pashynska, Y. O.; Marchuk, O. V.; Gulay, L. D.; Kaczorowski, D. Crystal structure and magnetic properties of $R_3Fe_{0.5}GeS_7$ (R = Y, La, Ce, Pr, Sm, Gd, Tb, Dy, Ho, Er and Tm). *J. Alloys Compd.* ***2014,*** *616, 243-249.*
11. Daszkiewicz, M.; Marchuk, O. V.; Gulay, L. D.; Kaczorowski, D. Crystal structure and magnetic properties of $R_3Mn_{0.5}GeS_7$ (R=Y, Ce, Pr, Nd, Sm, Gd, Tb, Dy, Ho and Er). *J. Alloys Compd.* ***2014,*** *610, 258-263.*
12. Daszkiewicz, M.; Pashynska, Y. O.; Marchuk, O. V.; Gulay, L. D.; Kaczorowski, D. Crystal structure and magnetic properties of $R_3Co_{0.5}GeS_7$ (R = Y, La, Ce, Pr, Nd, Sm, Gd, Tb, Dy, Ho, Er and Tm) and $R_3Ni_{0.5}GeS_7$(R = Y, Ce, Sm, Gd, Tb, Dy, Ho, Er and Tm). *J Alloys Compd.* ***2015,*** *647, 445-455.*
13. Huch, M. R.; Gulay, L. D.; Olekseyuk, I. D. Crystal structures of the $R_3Mg_{0.5}GeS_7$ (R=Y, Ce, Pr, Nd, Sm, Gd, Tb, Dy, Ho and Er) compounds. *J Alloys Compd.* ***2006,*** *424, 114-118.*
14. Iyer, A. K.; Yin, W.; Lee, E. J.; Lin, X.; Mar, A.; Lin, X.; Mar, A. Quaternary rare-earth sulfides $RE_3M_{0.5}GeS_7$ (RE=La–Nd, Sm; M=Co, Ni) and $Y_3Pd_{0.5}SiS_7$. *J. Solid State Chem.* ***2017,*** *250, 14-23.*
15. Jin, Z.; Li, Z.; Du, Y. Synthesis and the crystal structure of $La_6NiSi_2S_{14}$ and $La_6CoSi_2S_{14}$. *Yingyong Huaxue.* ***1985,*** *2, 42-46.*
16. Michelet, A.; Flahaut, J. Sur les composés du type $La_6MnSi_2S_{14}$. *C. R. Acad. Sci. Ser. C.* ***1969,*** *269 , 1203-1205.*
17. Strok, O.; Daszkiewicz, M.; Gulay, L. Crystal structure of $R_3Mg_{0.5}DSe_7$ (R = Ce, Pr; D = Si, Ge). *Chem. Met. Alloys.* ***2015,*** *8, 16-21.*
18. Sun, Y.-L.; Yang, C.; Guo, S.-P. Synthesis and crystal structure of a new quaternary sulfide $FeSm_6Si_2S_{14}$. *Jiegou Huaxue.* ***2013,*** *202, 269-275.*
19. Yin, W.; Wang, W.; Kang, L.; Lin, Z.; Feng, K.; Shi, Y.; Hao, W.; Yao, J.; Wu, Y. Ln_3FeGaQ_7: A new series of transition-metal rare-earth chalcogenides. *J. Solid State Chem.* ***2013,*** *202, 269-275.*
20. Zhou, Y.; Iyer, A. K.; Oliynyk, A. O.; Heyberger, M.; Lin, Y.; Qiu, Y.; Mar, A. O.-H. Quaternary rare-earth sulfides $RE_3M_{0.5}M'S_7$ (M = Zn, Cd; M′ = Si, Ge). *J. Solid State Chem.* ***2019,*** *278, 120914.*
21. Wu, L.-B.; Huang, F.-Q. Crystal structure of trilanthanum monosilver monosilicon heptasulfide, La_3AgSiS_7. *Z. für Krist. - New Cryst. Struct.* ***2005,*** *220, 327-328.*
22. Akopov, G.; Hewage, N. W.; Yox, P.; Viswanathan, G.; Lee, S. J.; Hulsebosch, L. P.; Cady, S. D.; Paterson, A. L.; Perras, F. A.; Xu, W.; Wu, K.; Mudryk, Y.; Kovnir, K. Synthesis-enabled exploration of chiral and polar multivalent quaternary sulfides. *Chem. Sci. J.* ***2021,*** *12, 14718-14730.*
23. Collin, G.; Laurelle, P. Structure cristalline de $La_6MnSi_2S_{14}$. *C. R. Acad. Sci. Ser. C.* ***1970,*** *270, 410-412.*
24. Gitzendanner, R. L.; Spencer, C. M.; DiSalvo, F. J.; Pell, M. A.; Ibers, J. A. Synthesis and Structure of a New Quaternary Rare-Earth Sulfide, $La_6MgGe_2S_{14}$, and the Related Compound $La_6MgSi_2S_{14}$. *J. Solid State Chem.* ***1997,*** *131, 399-404.*
25. Lin, F.; Luo, M.; Wang, R.; Che, X.; Huang, F. $La_6Cd_{0.75}Ga_2Q_{11.5}Cl_{2.5}$ (Q = S and Se): two new nonlinear optical chalcohalides with a large laser-induced damage threshold. *CrystEngComm.* ***2021,*** *23, 2133-2137.*
26. He, J.; Wang, Z.; Zhang, X.; Cheng, Y.; Gong, Y.; Lai, X.; Zheng, C.; Lin, J.; Huang, F. Synthesis, structure, magnetic and photoelectric properties of

$Ln_3M_{0.5}M'Se_7$ (Ln = La, Ce, Sm; M = Fe, Mn; M′ = Si, Ge) and $La_3MnGaSe_7$. *RSC Advances.* ***2015,*** *5, 52629-52635.*

27. Krause, L.; Herbst-Irmer, R.; Sheldrick, G. M.; Stalke, D. Comparison of silver and molybdenum microfocus X-ray sources for single-crystal structure determination. *J. Appl. Crystallogr.* ***2015,*** *48, 3-10.*
28. Sheldrick, G. M. *Shelxt*– Integrated Space-Group and Crystal-Structure Determination. *Acta Crystallogr. A..* ***2015,*** *71, 3-8.*
29. Hübschle, C. B.; Sheldrick, G. M.; Dittrich, B. ShelXle: a Qt graphical user interface for SHELXL. *J Appl. Crystallogr.* ***2011,*** *44, 1281-1284.*
30. Morrison, G.; zur Loye, H.-C. Simple Correction for the Sample Shape and Radial Offset Effects on SQUID Magnetometers: Magnetic Measurements on Ln_2O_3(Ln=Gd, Dy, Er) Standards. *J. Solid State Chem.* ***2015,*** *221, 334-337.*
31. Kubelka, P.; Munk, F. F. Ein Beittrag zur Optik der Farbanstriche. *Z. Technol. Phys.* ***1931,*** *593.*
32. Kurtz, S. K.; Perry, T. T. A Powder Technique for the Evaluation of Nonlinear Optical Materials. *J. Appl. Phys.* ***1968,*** *39, 3798-3813.*
33. Ok, K. M.; Chi, E. O.; Halasyamani, P. S. Bulk characterization methods for non-centrosymmetric materials: second-harmonic generation, piezoelectricity, pyroelectricity, and ferroelectricity. *Chem. Soc. Rev.* ***2006,*** *35, 710-717.*
34. Hatscher, S. T. U., W. Synthese Und Kristallstrukturen Von $Ln_3I(SiS_4)_2$ (LN=Pr, Nd, Sm, Tb). *Z. anorg. allg. Chem.* ***2001,*** *627, 2198.*
35. Hatscher, S. T.; Urland, W. Synthesis and structures of chloride thiosilicates with lanthanides $Ln_3Cl[SiS_4]_2$ (Ln = La, Ce, Pr). *Mater. Res. Bull.* ***2002,*** *37, 1239-1247.*
36. Vleck, V.; Hasbrouck, J. The theory of electric and magnetic susceptibilities. *Oxford University Press.* ***1965.***
37. Yoshitaka, M.; Yoshihiro, D.; Yukio, H. Crystal structures and magnetic properties of ternary sulfides $BaLn_2S_4$ (Ln = Sm, Gd-Lu). *J. Ceram. Soc. Japan.* ***2009,*** *117, 85-88.*
38. Shi, Y.-F.; Chen, Y.-k.; Chen, M.-C.; Wu, L.-M.; Lin, H.; Zhou, L.-J.; Chen, L. Strongest Second Harmonic Generation in the Polar R_3MTQ_7Family: Atomic Distribution Induced Nonlinear Optical Cooperation. *Chem. Mater.* ***2015,*** *27, 1876-1884.*
39. Poduska, K. M.; DiSalvo, F. J.; Min, K.; Halasyamani, P. S. Structure determination of La_3CuGeS_7 and $La3_{Cu}GeSe_7$. *J. Alloys Compd.* ***2002,*** *335, L5-L9.*
40. Yang, Y.; Chu, Y.; Zhang, B.; Wu, K.; Pan, S. Unique Unilateral-Chelated Mode-Induced d–p−π Interaction Enhances Second-Harmonic Generation Response in New Ln_3LiMS_7 Family. *Chem. Mater.* ***2021,*** *33, 4225-4230.*

Chapter 3:

1. Priyadarshini, P.; Sahoo, D.; Naik, R. A review on the optical properties of some germanium based chalcogenide thin films and their applications. *Opt. Quantum Electron.* ***2022,*** *54,*
2. Sahoo, D.; Naik, R. A review on the linear/nonlinear optical properties of Se doped chalcogenide thin films as potential optoelectronic applications. *J. Non-Cryst. Solids.* ***2022,*** *597, 121934.*
3. Kanatzidis, M. G. Discovery-Synthesis, Design, and Prediction of Chalcogenide Phases. *Inorg. Chem.* ***2017,*** *56, 3158-3173.*
4. Zhen, N.; Nian, L.; Li, G.; Wu, K.; Pan, S. A High Laser Damage Threshold and a Good Second-Harmonic Generation Response in a New Infrared NLO Material: $LiSm_3SiS_7$. *Crystals.* ***2016,*** *6, 121.*
5. Kamaya, N.; Homma, K.; Yamakawa, Y.; Hirayama, M.; Kanno, R.; Yonemura, M.; Kamiyama, T.; Kato, Y.; Hama, S.; Kawamoto, K.; Mitsui, A. A lithium superionic conductor. *Nat. Mater.* ***2001,*** *158, 682-686.*
6. Kanno, R.; Murayama, M. Lithium Ionic Conductor Thio-LISICON: The Li_2S-GeS_2-P_2S_5 System. *Nat. Mater.* ***2011,*** *148, A742.*
7. Iwanczyk, J. S.; Nygård, E.; Meirav, O.; Arenson, J.; Barber, W. C.; Hartsough, N. E.; Malakhov, N.; Wessel, J. C. Photon Counting Energy Dispersive Detector Arrays for X-ray Imaging. *IEEE Trans Nucl Sci.* ***2009,*** *56, 535-542.*
8. Rogalski, A. HgCdTe infrared detectro material: history, status and outlook. *Rep. Prog. Phys.* ***2005,*** *68, 2267-2336.*
9. Watanabe, S.; Ishikawa, S.-n.; Aono, H.; Takeda, S.; Odaka, H.; Kokubun, M.; Takahashi, T.; Nakazawa, K.; Tajima, H.; Onishi, M.; Kuroda, Y. High Energy Resolution Hard X-Ray and Gamma-Ray Imagers Using CdTe Diode Devices. *IEEE Trans. Nuc. Sci.* ***2009,*** *56, 777-782.*
10. Bera, T. K.; Jang, J. I.; Ketterson, J. B.; Kanatzidis, M. G. Strong second harmonic generation from the tantalum thioarsenates $A_3Ta_2AsS_{11}$ (A = K and Rb). *J. Am. Chem. Soc.* ***2009,*** *131, 75-77.*
11. Bera, T. K.; Jang, J. I.; Song, J. H.; Malliakas, C. D.; Freeman, A. J.; Ketterson, J. B.; Kanatzidis, M. G. Soluble semiconductors $AAsSe_2$ (A = Li, Na) with a direct-band-gap and strong second harmonic generation: a combined experimental and theoretical study. *J. Am. Chem. Soc.* ***2010,*** *132, 3484-3495.*
12. Lekse, J. W.; Moreau, M. A.; McNerny, K. L.; Yeon, J.; Halasyamani, P. S.; Aitken, J. A. Second-harmonic generation and crystal structure of the diamond-like semiconductors Li_2CdGeS_4 and Li_2CdSnS_4. *Inorg. Chem.* ***2009,*** *48, 7516-7518.*
13. Babo, J. M.; Choi, E. S.; Albrecht-Schmitt, T. E. Synthesis, structure, magnetism, and optical properties of $Cs_2Cu_3DyTe_4$. *Inorg. Chem.* ***2012,*** *51, 11730-11735.*
14. Caron, J. M.; Neilson, J. R.; Miller, D. C.; Llobet, A.; McQueen, T. M. Iron displacements and magnetoelastic coupling in the antiferromagnetic spin-ladder compound $BaFe_2Se_3$. *Phys. Rev. B.* ***2011,*** *84,*
15. King, A. A.; Breton, L. S.; Morrison, G.; Smith, M. D.; Liang, M.; Halasyamani, P. S.; Zur Loye, H.-C. Crystal Structures and Property Measurements of Rare Earth Magnesium Thiosilicates Synthesized via Flux Crystal Growth Utilizing the Boron Chalcogen Mixture (BCM) Method. *Inorg. Chem.* ***2023,*** *62, 7446-7452.*

16. Zhou, Y.; Iyer, A. K.; Oliynyk, A. O.; Heyberger, M.; Lin, Y.; Qiu, Y.; Mar, A. Quaternary rare-earth sulfides $RE_3M_{0.5}M'S_7$ (M = Zn, Cd; M′ = Si, Ge). *J. Solid State Chem.* ***2019,*** *278, 120914.*
17. Daszkiewicz, M.; Pashynska, Y. O.; Marchuk, O. V.; Gulay, L. D.; Kaczorowski, D. Crystal structure and magnetic properties of $R_3Fe_{0.5}GeS_7$ (R = Y, La, Ce, Pr, Sm, Gd, Tb, Dy, Ho, Er and Tm). *J. Alloys Compd.* ***2014,*** *616, 243-249.*
18. Daszkiewicz, M.; Pashynska, Y. O.; Marchuk, O. V.; Gulay, L. D.; Kaczorowski, D. Crystal structure and magnetic properties of $R_3Co_{0.5}GeS_7$ (R = Y, La, Ce, Pr, Nd, Sm, Gd, Tb, Dy, Ho, Er and Tm) and $R_3Ni_{0.5}GeS_7$ (R = Y, Ce, Sm, Gd, Tb, Dy, Ho, Er and Tm). *J. Alloys Compd.* ***2015,*** *647, 445-455.*
19. Gulay, L. D.; Olekseyuk, I. D.; Wołcyrz, M.; Stępień-Damm, J. The Crystal Structures of R_3CuSnS_7 (R = La-Nd, Sm, Gd-Ho). *Z. anorg. allg. Chem.* ***2005,*** *631, 1919-1923.*
20. Gulay, L. D.; Kaczorowski, D.; Pietraszko, A. Crystal structure and magnetic properties of $Ce_3CuSnSe_7$. *J. Alloys Compd.* ***2005,*** *403, 49-52.*
21. Guo, S. P.; Guo, G. C.; Wang, M. S.; Zou, J. P.; Xu, G.; Wang, G. J.; Long, X. F.; Huang, J. S. A series of new infrared NLO semiconductors, $ZnY_6Si_2S_{14}$, $Al_xDy_3(Si_{y)}Al_{1-y})S_7$, and $Al_{0.33}Sm_3SiS_7$. *Inorg. Chem.* ***2009,*** *48, 7059-7065.*
22. He, J.; Wang, Z.; Zhang, X.; Cheng, Y.; Gong, Y.; Lai, X.; Zheng, C.; Lin, J.; Huang, F. Synthesis, structure, magnetic and photoelectric properties of $Ln_3M_{0.5}M'Se_7$ (Ln = La, Ce, Sm; M = Fe, Mn; M′ = Si, Ge) and $La_3MnGaSe_7$. *RSC Advances.* ***2015,*** *5, 52629-52635.*
23. Iyer, A. K.; Yin, W.; Lee, E. J.; Lin, X.; Mar, A. Quaternary rare-earth sulfides $RE_3M_{0.5}GeS_7$ (RE=La–Nd, Sm; M=Co, Ni) and $Y_3Pd_{0.5}SiS_7$. *J. Solid State Chem.* ***2017,*** *250, 14-23.*
24. Melnychuk, K.; Marchuk, O.; Daszkiewicz, M.; Gulay, L. Crystal structure of novel $R_3Fe(Co, Ni)_{0.5}SnS_7$ (R = Y, La, Ce, Pr, Nd, Sm, Gd, Tb, Dy and Ho) compounds. *Struct. Chem.* ***2020,*** *31, 1945-1957.*
25. Akopov, G.; Hewage, N. W.; Yox, P.; Viswanathan, G.; Lee, S. J.; Hulsebosch, L. P.; Cady, S. D.; Paterson, A. L.; Perras, F. A.; Xu, W.; Wu, K.; Mudryk, Y.; Kovnir, K. Synthesis-enabled exploration of chiral and polar multivalent quaternary sulfides. *Chem. Sci.* ***2021,*** *12, 14718-14730.*
26. Krause, L.; Herbst-Irmer, R.; Sheldrick, G. M.; Stalke, D. Comparison of silver and molybdenum microfocus X-ray sources for single-crystal structure determination. *J Appl. Crystallogr.* ***2015,*** *48, 3-10.*
27. Sheldrick, G. M. *Shelxt*– Integrated Space-Group and Crystal-Structure Determination. *Acta Crystallogr. A.* ***2015,*** *71, 3-8.*
28. Hübschle, C. B.; Sheldrick, G. M.; Dittrich, B. ShelXle: a Qt graphical user interface for SHELXL. *J Appl. Crystallog.* ***2011,*** *44, 1281-1284.*
29. Morrison, G.; zur Loye, H.-C. Simple Correction for the Sample Shape and Radial Offset Effects on SQUID Magnetometers: Magnetic Measurements on Ln_2O_3(Ln=Gd, Dy, Er) Standards. *J. Solid State Chem.* ***2015,*** *221, 334-337.*
30. Collin G.; Laurelle, P. Structure cristalline de $La_6MnSi_2S_{14}$. *C. R. Acad. Sci. Ser. C.* ***1970,*** *270, 410-412.*
31. Collin G.; Laurelle, P. Structure de $La_6Cu_2Si_2S_{14}$. *Bull. Soc. Fr. Mineral. Cristallogr.* ***1971,*** *94, 175-176.*

32. Michelet, A.; Flahaut, J. Sur les composés du type $La_6MnSi_2S_{14}$. *C. R. Acad. Sci. Ser. C.* ***1969,*** *269 , 1203-1205.*